AD-A053 594 INTERMETRICS INC CAMBRIDGE MASS F/G 17/7
COMPARISON OF THREE VERTICAL CHANNEL DESIGNS FOR AN INTEGRATED --ETC(U)
DEC 77 W S WIDNALL, P K SINHA F33615-77-C-1044
UNCLASSIFIED IR-234 AFAL-TR-77-208 NL

| OF |
ADA
053594

END
DATE
FILMED
6-78
DDC

AFAL-TR-77-208

COMPARISON OF THREE VERTICAL CHANNEL DESIGNS FOR AN INTEGRATED GPS/INERTIAL NAVIGATION SYSTEM

Intermetrics, Incorporated
Cambridge, Massachusetts 02138

December 1977

TECHNICAL REPORT AFAL-TR-77-208

Interim Report for Period December 1976 to July 1977

Approved for Public Release; Distribution Unlimited

AIR FORCE AVIONICS LABORATORY
AIR FORCE WRIGHT AERONAUTICAL LABORATORIES
AIR FORCE SYSTEMS COMMAND
WRIGHT-PATTERSON AIR FORCE BASE, OHIO 45433

NOTICE

When Government drawings, specifications, or other data are used for any purpose other than in connection with a definitely related Government procurement operation, the United States Government thereby incurs no responsibility nor any obligation whatsoever; and the fact that the government may have formulated, furnished, or in any way supplied the said drawings, specifications, or other data, is not to be regarded by implication or otherwise as in any manner licensing the holder or any other person or corporation, or conveying any rights or permission to manufacture, use, or sell any patented invention that may in any way be related thereto.

This report has been reviewed by the Information Office (OI) and is releasable to the National Technical Information Service (NTIS). At NTIS, it will be available to the general public, including foreign nations.

This technical report has been reviewed and is approved for publication.

DAVID P. PAYNE
Project Engineer
Reference Systems Branch
Recon & Weap Del Div

RONALD L. RINGO, Chief
Reference Systems Branch
Reconnaissance & Weapon Delivery Div.

FOR THE COMMANDER

ROBERT E. DEAL, Asst Chief
Reconnaissance and Weapon
Delivery Division

"If your address has changed, if you wish to be removed from our mailing list, or if the addressee is no longer employed by your organization please notify AFAL/RWM *,W-PAFB, OH 45433 to help us maintain a current mailing list".*

Copies of this report should not be returned unless return is required by security considerations, contractual obligations, or notice on a specific document.

UNCLASSIFIED

SECURITY CLASSIFICATION OF THIS PAGE (When Data Entered)

REPORT DOCUMENTATION PAGE

READ INSTRUCTIONS BEFORE COMPLETING FORM

1. REPORT NUMBER: AFAL-TR-77-208	2. GOVT ACCESSION NO.
3. RECIPIENT'S CATALOG NUMBER	
4. TITLE (and Subtitle): Comparison of Three Vertical Channel Designs for an Integrated GPS/Inertial Navigation System.	5. TYPE OF REPORT & PERIOD COVERED: Interim Report Dec 1976 - July 1977,
6. PERFORMING ORG. REPORT NUMBER: IR-234	
7. AUTHOR(s): William S. Widnall and Prasun K. Sinha	8. CONTRACT OR GRANT NUMBER(s): F33615-77-C-1044
9. PERFORMING ORGANIZATION NAME AND ADDRESS: Intermetrics, Incorporated, 701 Concord Avenue, Cambridge, Massachusetts 02138	10. PROGRAM ELEMENT, PROJECT, TASK AREA & WORK UNIT NUMBERS: 666A
11. CONTROLLING OFFICE NAME AND ADDRESS: Reference Systems Branch, Reconnaissance & Weapons Delivery Division, Air Force Avionics Laboratory, Wright Patterson Air Force Base, Ohio 45433	12. REPORT DATE: December 1977
	13. NUMBER OF PAGES: 86 (12) 84 p.
14. MONITORING AGENCY NAME & ADDRESS (if different from Controlling Office)	15. SECURITY CLASS. (of this report): UNCLASSIFIED
	15a. DECLASSIFICATION/DOWNGRADING SCHEDULE

16. DISTRIBUTION STATEMENT (of this Report)

Approved for Public Release; Distribution Unlimited

17. DISTRIBUTION STATEMENT (of the abstract entered in Block 20, if different from Report)

N/A

18. SUPPLEMENTARY NOTES

N/A

19. KEY WORDS (Continue on reverse side if necessary and identify by block number)

Kalman Filter
Vertical Channel
Inertial Navigation Systems
Global Positioning System
Integrated Navigation Systems
Barometric Altimeter Error Models
LN-15 INS Error Model

20. ABSTRACT (Continue on reverse side if necessary and identify by block number)

The Integrated GPS/Inertial (IGI) Simulator is utilized to explore design issues associated with the vertical channel of a GPS/baro/inertial navigation system. The assumed navigation system includes a local-level wander azimuth inertial navigation system with associated barometric altimeter for stabilizing the vertical channel, a Global Positioning System (GPS) pseudo range and range-rate receiver, and a navigation computer hosting a

DD FORM 1 JAN 73 1473 EDITION OF 1 NOV 65 IS OBSOLETE

UNCLASSIFIED

SECURITY CLASSIFICATION OF THIS PAGE (When Data Entered)

388 863

Block 20 (Contd.)

Kalman filter to integrate the baro/inertial and GPS data. The simulated flight path is an F-4 high dynamic tactical mission profile. Of particular interest in evaluating vertical channel performance is a seven minute period during which jamming prevents the use of GPS measurements. Three Kalman filter designs are evaluated. Filter A has 17 states including two states modeling the altimeter bias and scale factor error. This filter provides the smallest peak altitude and vertical velocity errors. Filter B has 16 states including one state modeling altimeter bias. This filter provides the second best performance. Filter C has 16 states including one state modeling altimeter scale factor error. This filter provides the worst performance, in fact during the period of jamming the vertical velocity errors are larger than the vertical velocity errors of the no-filter baro inertial system. During un-jammed periods, all three designs provide nearly identical performance.

FOREWORD

This technical report was prepared by Drs. William S. Widnall and Prasun K. Sinha of Intermetrics, Incorporated, Cambridge, Massachusetts. The work was sponsored by the Air Force Avionics Laboratory, Air Force Systems Command, Wright-Patterson Air Force Base, Ohio 45433 under contract F33615-77-C-1044 of Project 666A. The initial AFAL project manager was Major Kenneth A. Myers. The subsequent project manager was Capt. David P. Payne (AFAL/RWA-1) with project engineer Capt. Ronald R. Butler. The research reported was conducted from December 1976 to July 1977. The report was initially submitted to the AFAL on 27 July 1977. The manuscript was prepared by Eileen Martin and Marcia Brehm at Intermetrics.

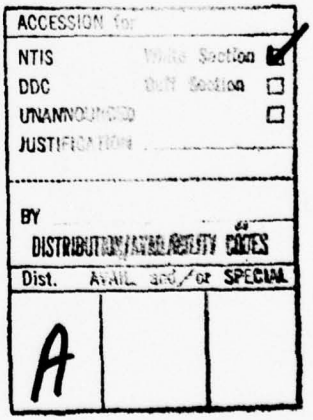

TABLE OF CONTENTS

		PAGE
I.	INTRODUCTION	1
	1.1 Background	1
	1.2 Vertical Channel Design Issues	1
	1.3 Outline of Report	3
II.	SIMULATION ERROR MODELS AND TRAJECTORY	5
	2.1 Error State Propagation Equations	5
	2.2 Vertical Channel Error Model	14
	2.3 GPS Measurements Error Model	18
	2.4 F4 Aircraft Trajectory	21
	2.5 Baro-Inertial Navigation Errors	21
III.	FILTER ERROR MODELS	33
	3.1 Inertial and Clock Error Models	33
	3.2 Two-State Altimeter Error Model	40
	3.3 Bias Single State Altimeter Error Model	43
	3.4 Scale Factor Single State Altimeter Error Model	43
	3.5 Measurements Error Model	45
IV.	INTEGRATED GPS/INERTIAL PERFORMANCE	47
	4.1 Horizontal Position and Velocity Errors	48
	4.2 Vertical Channel Errors	54
	4.3 Attitude and Gyro Drift Errors	62
	4.4 Clock Phase and Frequency Errors	67
V.	SUMMARY AND CONCLUSIONS	71
	REFERENCES	75

LIST OF ILLUSTRATIONS

FIGURE		PAGE
2-1	Third Order Baro-Stabilized Vertical Channel Error Model	14
2-2	User Clock Error Model	20
2-3	F-4 Mission Ground Track	22
2-4	F-4 Mission Altitude Profile	23
2-5	F-4 Mission Yaw Profile	24
2-6	INS Horizontal Position Errors	28
2-7	INS Horizontal Velocity Errors	29
2-8	INS Altitude and Vertical Velocity Errors	30
2-9	X and Y Accelerometer Misalignment from East and North	31
3-1	Clock Error Model of the Filter	38
4-1	GPS/Inertial East Position Errors	49
4-2	GPS/Inertial North Position Errors	50
4-3	GPS/Inertial East Velocity Errors	52
4-4	GPS/Inertial North Velocity Errors	53
4-5	GPS/Inertial Altitude Errors for Case A (Expanded Scale)	55
4-6	GPS/Inertial Altitude Errors	56
4-7	GPS/Inertial Vertical Velocity Errors	57
4-8	Filter A Altimeter Bias and Scale Factor Errors	58
4-9	Filter B Altimeter Bias Error	61
4-10	Filter C Altimeter Effective Scale Factor Error	61
4-11	GPS/Inertial East Attitude Errors	64
4-12	GPS/Inertial North Attitude Errors	65
4-13	GPS/Inertial Azimuth Errors	66
4-14	Clock Phase Errors	68

LIST OF ILLUSTRATIONS (Contd.)

FIGURE		PAGE
4-15	Clock Frequency Errors	69
4-16	Clock Phase Errors for Case C (Expanded Scale)	70

TABLES

TABLE		PAGE
2-1	Error Model State Variables	6
2-2a	Fundamental Matrix of the General Error Differential Equations for the Basic Errors	8
2-2b	Fundamental Matrix for LN-15 Vertical Channel, Partition of First Eleven State Variables (Added to Fundamental Elements in Part a)	8
2-2c	Fundamental Matrix, Non-Zero Partitions of Gyro Error State Variables	9
2-2d	Fundamental Matrix, Partitions of Accelerometer, Altimeter, and Gravity Disturbance State Variables	9
2-2e	Non-Zero Partitions of User Clock State Variables	10
2-3	Notation Used in Tables 2-2 and 2-4	11
2-4	Simulation Noise Density Matrix, Non Zero Elements	12
2-5	Error Source Initial Values and Statistics	13
3-1	Filter State Variables	34
4-1	Altimeter Bias True Values and Filter Estimates - Case A	59

SECTION I
INTRODUCTION

1.1 Background

The Global Positioning System (GPS) is a satellite navigation system currently under development by the U. S. Department of Defense. The Air Force Avionics Laboratory (AFAL) is participating in this program with the development of a Generalized Development Model (GDM) of GPS User Equipment. The AFAL GDM will serve as a flight test bed to evaluate high anti-jam system techniques for military applications and to expand the technology base for GPS User Equipment.

In support of the AFAL GPS development responsibilities, personnel at the AFAL have developed a simulation program for evaluating the performance of integrated GPS/inertial navigation systems. This simulator, called the IGI (Integrated GPS/Inertial) Simulator, provides a direct time domain simulation of the errors in an inertial navigation system and the errors in GPS measurements. It provides the framework for evaluating alternate sequential filter designs for mixing the GPS and inertial data to provide the desired accurate navigation outputs. A paper by K. A. Myers and R. R. Butler of the AFAL provides an introduction to the IGI Simulator[1]. An overview of the simulator design is provided plus some simulation results for a six-hour flight of a C5A.

The AFAL has contracted with Intermetrics to provide additional analysis, simulation, and software support. One of the tasks undertaken by Intermetrics includes vertical channel analysis and simulation using the IGI simulator. This report summarizes the results of this analysis.

1.2 Vertical Channel Design Issues

The vertical channel of a pure inertial navigator is known to be unstable. Assuming gravity is computed as a function of the indicated altitude, it can be shown that the positive feedback caused by the gravity computation error produces exponential growth in the errors in the

indicated vertical velocity and altitude. Accordingly, it is common design practice to stabilize the vertical channel of a three-axis cruise navigator by utilizing some external source of altitude information, usually barometric altimeter data.

The initial IGI Simulator developed by Myers and Butler incorporates an error model for the Litton LN-15 baro-inertial navigator. This error model was derived and documented in a report by Widnall and Grundy[2]. The LN-15 employs a local-level wander-azimuth mechanization. In the vertical channel, the inertial and barometric data are blended by a constant gain set of differential equations. The vertical channel follows the high frequency maneuvering of the aircraft as measured by the z accelerometer; however, the long term steady state solution in the vertical channel is for the indicated altitude to converge to the baro-indicated altitude.

In a subsonic aircraft the two largest sources of error in the baro-indicated altitude may be the standard setting error and a scale factor error. The standard setting error is related to the variation in the height of a constant pressure surface (the pattern of "highs" and "lows"). If the altimeter feeding the INS is left set at standard pressure during an entire flight, then the one-sigma level of this variation can be of the order of 500 feet. The scale factor error is related to the temperature of the atmosphere differing from the standard day temperature profile. On a cold day, the atmosphere shrinks and a particular altimeter reading is obtained at a lower true altitude. The reverse occurs on a hot day. A typical scale factor error is 3%. At 30,000 feet altitude this would be a significant error of 900 feet. Both the standard setting error and the scale factor error were included in the initial version of the IGI Simulator.

In the design of practical real-time recursive filters to blend inertial navigation and other (in this case GPS measurement) data, one cannot utilize an "optimal" filter. That is, one cannot have modeled in the filter all the sources of error in the navigation data. One designs a "sub-optimal" filter, which has many fewer states than the sources of error. The initial IGI simulator included fifty-two states modeling sources of inertial and GPS error and their propagation dynamics. The suboptimal filter which blended the GPS and inertial data had sixteen states.

One of the sixteen states of the filter modeled the altimeter error of the baro-inertial system. To minimize the number of states in the filter only one altimeter error state was used. This state was defined to be a scale factor error and was modeled in the filter as a random constant. Myers and Butler reported[1] that this vertical channel design was not satisfactory. If the truth model contained both the standard setting error and a scale factor error of only 1%, then the filter diverged from correct estimates of vertical velocity, altitude, latitude, and longitude.

These initial results with the IGI simulator raised issues concerning vertical channel design associated with the choice of state variables in the recursive filter and use of these state variables to model all significant related sources of error. Should two-state variables be used in the filter to model altimeter error, or is one sufficient? If only one state is used, should it be a bias-like error model or should it be scale-factor error model? How can an assumed white noise driving a single error state be used to model the effects of other sources of error? These issues are addressed in this report.

1.3 Outline of Report

The IGI Simulator is used to evaluate alternate Kalman filter vertical channel designs. Section II summarizes the truth model provided by the simulator. The error models of the baro-inertial navigator and of the GPS measurements are presented. A F4 aircraft trajectory has been selected to drive the error models. This trajectory is also described in Section II. The baro-inertial navigation errors produced by the assumed sources of error and by the assumed trajectory are plotted and presented.

Section III presents a basic recursive (Kalman) filter for blending the inertial navigation and GPS measurement data. Then three alternate vertical channel filter designs are presented.

1. Filter A has two states representing the altimeter sources of error, an altimeter bias state and an altimeter scale factor error state.

2. Filter B has a single altimeter error state, an altimeter bias state.

3. Filter C has a single altimeter error state, a scale factor error state.

Appropriate expressions are developed for the spectral densities of the assumed noises driving these states. These noises model the important sources of error that have not been included as states.

Section IV presents the results of running each of these three filter designs in the IGI simulator with the same truth model for the errors and with the same F4 trajectory. The comparative performance is discussed.

Conclusions are presented in Section V.

SECTION II

SIMULATION ERROR MODELS AND TRAJECTORY

2.1 Error State Propagation Equations

The IGI simulator has organized the error models into a system of linear first order stochastic differential equations

$$\dot{\underline{x}} = F(t)\ \underline{x} + \underline{w} \qquad (2\text{-}1)$$

where $\underline{x}$ is the state vector, F is the fundamental matrix, and $\underline{w}$ is a vector of white noise disturbances.

Fifty four state variables are included in the state vector, as shown in Table 2-1. The first nine state variables are the basic position, velocity, and attitude errors common to all three-axis inertial navigators. State 10 is the altimeter scale factor error. State 11 is the vertical acceleration error variable of the third-order baro-inertial vertical channel of the LN-15. State 12 is the GPS user equipment clock phase error. State 13 is one of the user clock frequency error states. States 14, 15, and 16 are the gyro g-insensitive drift rates. These first sixteen states have some correspondence to the states of the sixteen state filter evaluated by Myers and Butler in Ref. [1]. This ordering of the states was chosen in Ref. [1] to emphasize this correspondence, and this ordering is retained here.

States 17 through 34 are additional gyro-related sources of error. States 35 through 46 are accelerometer sources of error. State 47 is the altimeter zero setting error. States 48, 49, and 50 are the deflections of gravity and gravity anomaly. States 51 and 52 are additional user clock error states. States 53 and 54 are two additional sources of altimeter error, the coefficient of static pressure measurement error, and the altimeter lag. The first 52 state variables are the same as selected by Myers and Butler in Ref. [1]. States 53 and 54 have been added in this study to provide greater fidelity for the altimeter error model.

Table 2-1 Error Model State Variables

Basic Inertial Navigation Errors

1. $\delta\lambda$ Error in east longitude
2. δL Error in north latitude
3. δh Error in altitude
4. δv_e Error in east velocity
5. δv_n Error in north velocity
6. δv_z Error in vertical velocity
7. ϵ_e Attitude error east component
8. ϵ_n Attitude error north component
9. ϵ_z Attitude error up component

Barometric Altimeter Error

10. e_{hsf} Altimeter scale factor error

Vertical Channel Error Variable

11. $\hat{\delta a}$ Vertical acceleration error variable in altitude channel

Clock Errors

12. δt_u User clock phase error
13. $\dot{\delta t}_{bu}$ User clock frequency bias

G-Insensitive Gyro Drift

14. DX_f X gyro drift rate
15. DY_f Y gyro drift rate
16. DZ_f Z gyro drift rate

G-Sensitive Gyro Drift Coefficients

17. DX_x X gyro input axis g-sensitivity
18. DX_y X gyro spin axis g-sensitivity
19. DY_x Y gyro spin axis g-sensitivity
20. DY_y Y gyro input axis g-sensitivity
21. DZ_y Z gyro spin axis g-sensitivity
22. DZ_z Z gyro input axis g-sensitivity

G^2-Sensitive Gyro Drift Coefficients

23. DX_{xy} X gyro spin-input g^2-sensitivity
24. DY_{xy} Y gyro spin-input g^2-sensitivity
25. DZ_{yz} Z gyro spin-input g^2-sensitivity

Gyro Scale Factor Errors

26. GSF_x X gyro scale factor error
27. GSF_y Y gyro scale factor error
28. GSF_z Z gyro scale factor error

Gyro Input Axis Misalignments

29. XG_y X gyro input axis misalignment about Y
30. XG_z X gyro input axis misalignment about Z
31. YG_x Y gyro input axis misalignment about X
32. YG_z Y gyro input axis misalignment about Z
33. ZG_x Z gyro input axis misalignment about X
34. ZG_y Z gyro input axis misalignment about Y

Accelerometer Biases

35. AB_x X accelerometer bias
36. AB_y Y accelerometer bias
37. AB_z Z accelerometer bias

Accelerometer Scale Factor Errors

38. ASF_x X accelerometer scale factor error
39. ASF_y Y accelerometer scale factor error
40. ASF_z Z accelerometer scale factor error

Accelerometer Input Axis Misalignments

41. XA_y X accelerometer input axis misalignment about Y
42. XA_z X accelerometer input axis misalignment about Z
43. YA_x Y accelerometer input axis misalignment about X
44. YA_z Y accelerometer input axis misalignment about Z

Accelerometer Input Axis Misalignments (Cont.)

45. ZA_x Z accelerometer input axis misalignment about X
46. ZA_y Z accelerometer input axis misalignment about Y

Additional Barometric Altimeter Error

47. e_{po} Error due to variation in altitude of a constant pressure surface

Gravity Deflections and Anomaly

48. δg_e East deflection of gravity
49. δg_n North deflection of gravity
50. δg_z Gravity anomaly

Additional Clock Errors

51. $\ddot{\delta t}_{bu}$ Clock aging bias
52. $\dot{\delta t}_{ru}$ Clock random frequency bias

Additional Barometric Altimeter Errors

53. c_{sp} Coefficient of static pressure measurements
54. τ_b Altimeter lag

Non-zero elements of partitions of the fundamental matrix are presented in Table 2-2, parts a, b, c, d, and e. Part a is the upper left nine by nine partition of the general INS error differential equations governing position, velocity, and attitude errors of any three axis INS. Part b gives the added elements in the upper left 11 by 11 partition peculiar to the baro-inertial LN-15 and its third order vertical channel mechanization. Part c identifies the non-zero elements of the columns associated with the gyro error sources. Part d identifies the non-zero elements of the columns associated with the accelerometer, gravity, and additional altimeter error sources. Part e gives the partitions associated with the four clock error states.

Table 2-3 defines the notation used in the fundamental matrix elements of Table 2-1 and in the noise spectral density matrix elements of Table 2-4.

Table 2-4 identifies the non-zero elements of the noise density matrix. Only some of the elements on the main diagonal are chosen to be non-zero in this error model.

Error source initial values and statistics are summarized in Table 2-5. The error sources here are grouped by model type: random walks, first order Markov processes, and random constants. For the random walks, the initial values of the states are given plus the noise spectral density of the driving noises. (Clock phase error is included here for convenience, although it is not simply a random walk.) For the first-order Markov processes, the one-sigma values and the inverse correlation times are given. The initial conditions for these processes have arbitrarily been chosen to be the positive one-sigma value. For the random constants, the selected values are generally the positive one-sigma value for each error source, except that in the case of gyro and accelerometer input axis misalignments both positive and negative values have been used to break up the orthogonality of the instruments.

The initial value for the z (azimuth) gyro g-insensitive drift rate (state 16) of -.295°/hr when combined with the z gyro sensitivity to z specific force (state 22) of 0.300°/hr/g in a one-g field produces a net initial z gyro drift rate of .005°/hr.

Ref. [3] presents the state vector, the fundamental matrix, the driving noise spectral densities, and the initial conditions used in generating the earlier results reported in Ref. [1]. Some of the changes made for this report include: two additional barometric altimeter error states (states 53 and 54) have been included. The definition of state 16 has

		$\delta\lambda$	δL	δh	δv_e	δv_n	δv_z	ε_e	ε_n	ε_z
		1	2	3	4	5	6	7	8	9
$\dot{\delta\lambda}$	1	0	$\rho_z/\cos L$	$-\rho_n/(R\cos L)$	$1/(R\cos L)$	0	0			
$\dot{\delta L}$	2	0	0	ρ_e/R	0	$1/R$	0		0	
$\dot{\delta h}$	3	0	0	0	0	0	1			
$\dot{\delta v}_e$	4	0	F_{42}	F_{43}	F_{44}	$(\omega_z+\Omega_z)$	$-(\omega_n+\Omega_n)$	0	$-f_z$	f_n
$\dot{\delta v}_n$	5	0	F_{52}	F_{53}	$-2\,\omega_z$	$-k_z$	ρ_e	f_z	0	$-f_e$
$\dot{\delta v}_z$	6	0	$-2\,\Omega_z v_e$	F_{63}	$2\,\omega_n$	$-2\,\rho_e$	0	$-f_n$	f_e	0
$\dot{\varepsilon}_e$	7	0	0	$-\rho_e/R$	0	$-1/R$	0	0	ω_z	$-\omega_n$
$\dot{\varepsilon}_n$	8	0	$-\Omega_z$	$-\rho_n/R$	$1/R$	0	0	$-\omega_z$	0	ω_e
$\dot{\varepsilon}_z$	9	0	F_{92}	$-\rho_z/R$	$\tan L/R$	0	0	ω_n	$-\omega_e$	0

Table 2-2a

Fundamental Matrix of the General Error Differential Equations for the Basic Errors

		$\delta\lambda$	δL	δh	δv_e	δv_n	δv_z	ε_e	ε_n	ε_z	e_{haf}	δs
		1	2	3	4	5	6	7	8	9	10	11
$\dot{\delta\lambda}$	1										0	0
$\dot{\delta L}$	2					0			0		0	0
$\dot{\delta h}$	3			$-k_1$							$k_1 h$	0
$\dot{\delta v}_e$	4										0	0
$\dot{\delta v}_n$	5					0			0		0	0
$\dot{\delta v}_z$	6			$-k_2$							$k_2 h$	-1
$\dot{\varepsilon}_e$	7											
$\dot{\varepsilon}_n$	8		0			0			0		0	0
$\dot{\varepsilon}_z$	9											
$\dot{e}_{haf}$	10	0	0	0							0	0
$\dot{\varepsilon}_a$	11	0	0	k_3		0			0		$-k_3 h$	0

Table 2-2b

Fundamental Matrix for LN-15 Vertical Channel, Partition of First Eleven State Variables (Added to Fundamental Elements in Part a)

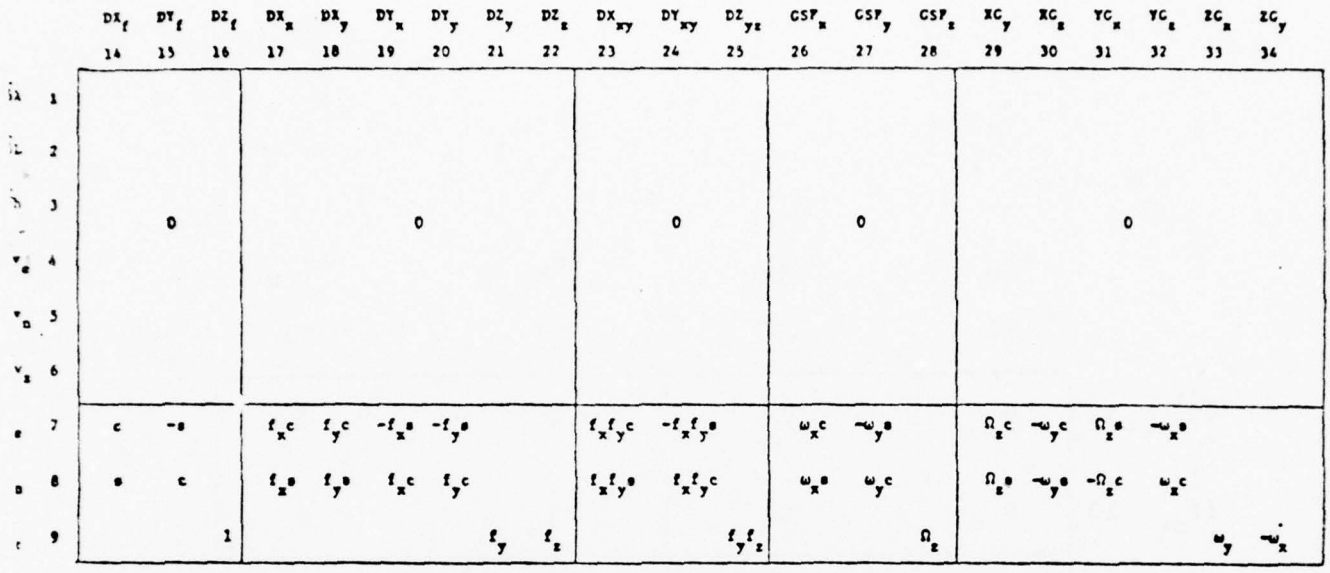

Table 2-2c

Fundamental Matrix, Non-Zero Partitions

of Gyro Error State Variables

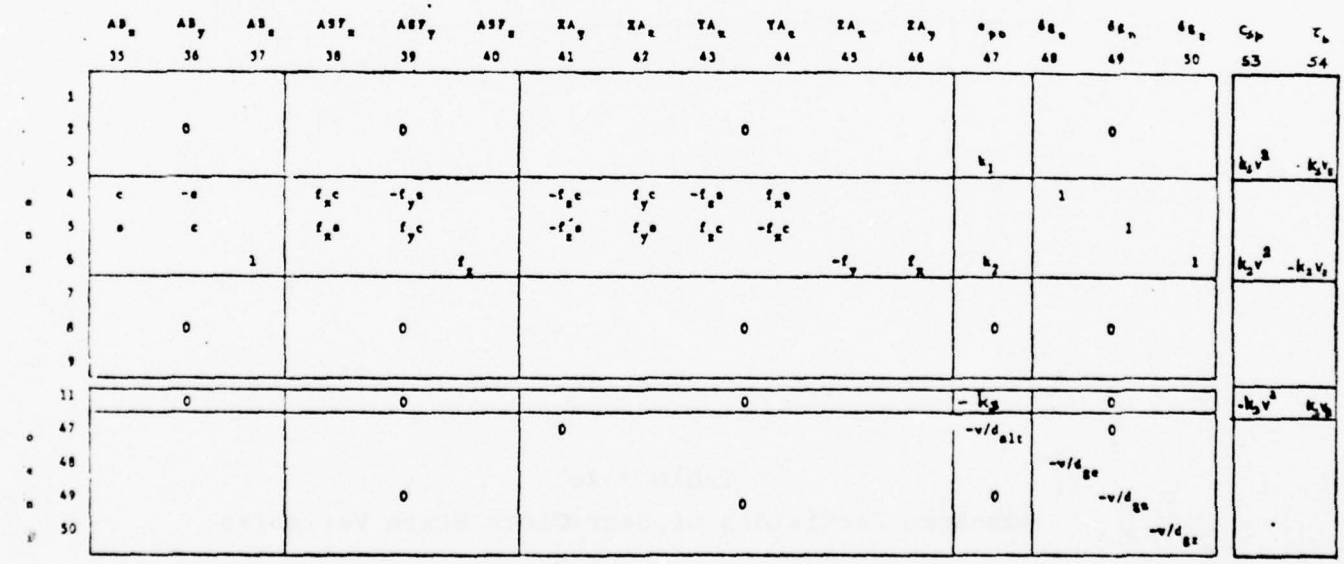

Table 2-2d

Fundamental Matrix, Partitions of Accelerometer,

Altimeter, and Gravity Disturbance State Variabes

		δt_u	$\dot{\delta t}_{bu}$	$\ddot{\delta t}_{bu}$	$\dot{\delta t}_{ru}$
		12	13	51	52
$\dot{\delta t}_u$	12	0	1	0	1
$\dot{\delta t}_{bu}$	13	0	0	1	0
$\ddot{\delta t}_{bu}$	51	0		0	0
$\dot{\delta t}_{ru}$	52			0	$-\beta_{tru}$

Table 2-2e
Non-Zero Partitions of User Clock State Variables

L	Latitude of vehicle
Ω	Earth rotation rate
R	Earth radius
g	Magnitude of gravity vector
v_e, v_n, v_z	Components of vehicle velocity with respect to earth
f_e, f_n, f_z	Components of specific force
$\Omega_n = \Omega \cos L$ $\Omega_z = \Omega \sin L$	Components of earth rate
$\rho_e = -v_n/R$ $\rho_n = v_e/R$ $\rho_z = v_e \tan L/R$	Components of angular velocity of E-N-Z frame with respect to earth
$\omega_e = \rho_e$ $\omega_n = \rho_n + \Omega_n$ $\omega_z = \rho_z + \Omega_z$	Components of angular velocity of E-N-Z frame with respect to inertial space
$k_z = v_z/R$	
$F_{42} = 2(\Omega_n v_n + \Omega_z v_z) + \rho_n v_n/\cos^2 L$	
$F_{43} = \rho_z \rho_e + \rho_n k_z$	
$F_{44} = -\rho_e \tan L - k_z$	
$F_{52} = -2 \Omega_n v_e - \rho_n v_e/\cos^2 L$	
$F_{53} = \rho_n \rho_z - \rho_e k_z$	
$F_{63} = 2g/R - (\rho_n^2 + \rho_e^2)$	
$F_{92} = \omega_n + \rho_z \tan L$	
k_1, k_2, k_3	Coefficients in altitude channel baro-inertial loop
c	cos α, cosine of the wander angle
s	sin α, sine of the wander angle
f_x, f_y, f_z	Components of specific force along the LN-15 x,y,z axes
ω_x, ω_y	Components of angular velocity of the E-N-Z frame with respect to inertial space along the LN-15 x,y axes
Ω_z	Up component of earth rate
h	Vehicle altitude
v	Vehicle ground speed
d_{alt}	Correlation distance of altimeter error
d_{ge}, d_{gn}, d_{gz}	Correlation distances of gravity deflections and anomaly
σ_{alt}	1σ amplitude of altimeter error e_{po}
σ_{ge}, σ_{gn}, σ_{gz}	1σ amplitude of gravity disturbances
σ_{tru}	1σ amplitude of clock random frequency error $\delta\dot{t}_{ru}$
β_{tru}	Inverse correlation time of clock random frequency error

Table 2-3 Notation Used in Tables 2-2 and 2-4

Table 2-4 Simulation Noise Density Matrix, Non Zero Elements

Diagonal Element	State Variable	Noise Density
12	δ_{tu}	N_{tu}
14	DX_f	N_{DXf}
15	DY_f	N_{DYf}
16	DZ_f	N_{DZf}
35	AB_x	N_{ABx}
36	AB_y	N_{ABy}
37	AB_z	N_{ABz}
47	e_{po}	$N_{epo} = 2\,\sigma^2_{alt}\ v/d_{alt}$
48	δg_e	$N_{ge} = 2\,\sigma^2_{ge}\ v/d_{ge}$
49	δg_n	$N_{gn} = 2\,\sigma^2_{gn}\ v/d_{gn}$
50	δg_z	$N_{gz} = 2\,\sigma^2_{gz}\ v/d_{gz}$
52	$\dot{\delta t}_{ru}$	$N_{tru} = 2\,\sigma^2_{tru}\ \beta_{tru}$

Table 2-5

Error Source Initial Values and Statistics

RANDOM WALKS $\dot{x} = w$			
State Variable Number	Error Source	Initial Value	Noise Spectral Density N
14, 15	X,Y (level) gyro drift rates	.003°/hr	$(.003°/hr)^2/hr$
16	Z (azimuth) gyro drift rate	-.295°/hr	$(.005°/hr)^2/hr$
12	Clock Phase Error	1000 ft.	$1\ ft^2/sec$
35, 36	X,Y (horizontal) accelerometer biases	50 μg	$(10\ \mu g)^2/hr$
37	Z (altitude) accelerometer bias	100 μg	$(10\ \mu g)^2/hr$

FIRST ORDER MARKOV PROCESSES $\dot{x} = -\beta x + w;\ N_w = 2\beta\sigma^2$			
State Variable Number	Error Source	Initial and 1σ Value	Inverse Correlation Time β
47	Barometric altimeter time-varying error	500 ft.	v/(250 n.mi.)
48	East deflection of gravity	26 μg	v/(10 n.mi.)
49	North deflection of gravity	17 μg	v/(10 n.mi.)
50	Gravity anomaly	35 μg	v/(60 n.mi.)
52	Clock random frequency	10 ft/sec	1/(7200 sec)

RANDOM CONSTANTS $\dot{x} = 0$		
State Variable Number	Error Source	Initial Value
17 to 22	G-sensitive gyro drift coefficients	0.3°/hr/g
23 to 25	G^2-sensitive gyro drift coefficients	$0.04°/hr/g^2$
26, 27	X,Y gyro scale factor errors	300 ppm
28	Z gyro scale factor error	1,000 ppm
29 to 34	Gyro input axis misalignments	±40 arc sec
38 to 40	Accelerometer scale factor errors	150 ppm
42, 44	X, Y accelerometer input axis misalignment about Z	±180 arc sec
41, 43 45, 46	Other accelerometer input axis misalignments	±30 arc sec
10	Barometric altimeter scale factor error	0.03
51	Clock aging bias error	$2.0 \times 10^{-7}\ ft/sec^2$
13	Clock frequency bias initial condition	1.0 ft/sec
53	Coefficient of Static Pressure Measurement Error	$\frac{1.54 \times 10^{-4}\ ft}{(ft/sec)^2}$
54	Barometric time delay	0.25 secs

been changed so that the state is the g-insensitive (free-fall) z gyro drift rate rather than the drift rate during one-g of z specific force. Similarly the definition of state 37 has been changed so that the state is the free fall z accelerometer bias rather than the accelerometer bias during one-g of z specific force. The definitions are now consistent with those used in Ref. [2]. The spectral density of the noise driving the clock phase error (state 12) has been reduced from 100 to 1 ft^2/sec. The one-sigma value of the first-order Markov clock random frequency (state 52) has been increased from 10^{-6} to 10 ft/sec, and its correlation time has been lengthened from 1800 sec to 7200 sec. Some of the gyro and accelerometer input axis misalignments were changed to negative values to break up the orthogonality of the instruments. The first order Markov processes are now started at positive one-sigma values rather than at zero.

2.2 Vertical Channel Error Model

Of primary concern in this analysis is the performance of the vertical channel of the integrated GPS/inertial navigation. Some discussion of the sources of error in the vertical channel of a baro/inertial navigator therefore is in order.

A block diagram of the error equations of the third-order LN-15 vertical channel is shown in Figure 2-1.

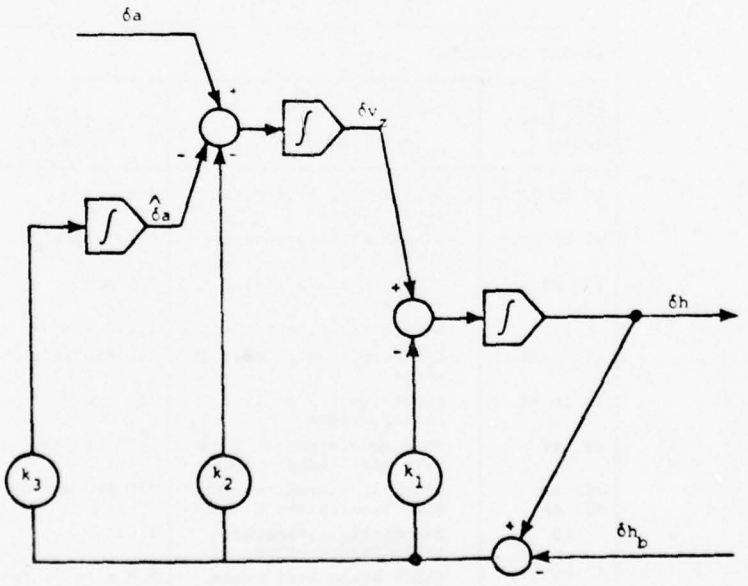

Figure 2-1 Third Order Baro-Stabilized Vertical Channel Error Model

The closed-loop altitude error δh, the vertical velocity error δv_z, and the LN-15 vertical acceleration error estimate variable $\delta\hat{a}$ are governed by

$$\dot{\delta h} = \delta v_z - k_1(\delta h - \delta h_b) \tag{2-2}$$

$$\dot{\delta v}_z = \delta a - k_2(\delta h - \delta h_b) - \delta\hat{a} \tag{2-3}$$

$$\dot{\delta\hat{a}} = k_3(\delta h - \delta h_b) \tag{2-4}$$

The values of the loop gains k_1, k_2, and k_3 used in the LN-15 are

$$k_1 = 3.0 \times 10^{-2} \text{ sec}^{-1}$$
$$k_2 = 3.0 \times 10^{-4} \text{ sec}^{-2}$$
$$k_3 = 1.0 \times 10^{-6} \text{ sec}^{-3}$$

This set of gains results in a stable altitude channel with a characteristic time constant of 100 secs.

The variable δa represents the inertial vertical acceleration error due to vertical accelerometer bias (AB_z), vertical accelerometer scale factor error (ASF_z), vertical accelerometer misalignments (ZA_x and ZA_y) about the platform x and y (level) axes, gravity anomaly δg_z, gravity computation error $(2g/R)\delta h$, and platform misalignments ε_e and ε_n, plus other sources.

$$\delta a = AB_z + f_z\, ASF_z - f_y\, ZA_x + f_x\, ZA_y + \delta g_z + \frac{2g}{R}\,\delta h$$
$$- f_n\, \varepsilon_e + f_e\, \varepsilon_n + \ldots \tag{2-5}$$

See row six of the fundamental matrix to identify all the terms.

δh_b represents the baro altimeter error and is the sum of altimeter error due to altimeter bias (e_{p_o}), altimeter scale factor (e_{hsf}), static pressure measurement error (c_{sp}) and altimeter lag (τ_b) when the aircraft climbs or descends

$$\delta h_b = e_{p_o} + h\, e_{hsf} + c_{sp}\, v^2 - \tau_b\, v_z \qquad (2\text{-}6)$$

where h is aircraft altitude, v is aircraft speed, and v_z is the vertical velocity.

The altimeter bias e_{p_o}, or standard setting error, or variation in height of a constant pressure surface changes slowly with time due primarily to the aircraft motion through the weather pattern and to a lesser extent due to the motion of the weather system. The rms variation of the altitude of the constant pressure surface has a bounded magnitude. This error is modeled as a first order Markov process given by

$$\dot{e}_{p_o} = -\omega_{alt}\, e_{p_o} + w_{p_o} \qquad (2\text{-}7)$$

$$\omega_{alt} = v/d_{alt} \qquad (2\text{-}8)$$

$$N_{alt} = 2\, \omega_{alt}\, \sigma_{alt}^2 \qquad (2\text{-}9)$$

where

d_{alt} = correlation distance of the weather system

σ_{alt} = standard deviation of the variation in altitude of a constant pressure surface

N_{alt} = power spectral density of the white noise process w_{p_o}

v = aircraft speed

The altimeter scale factor e_{hsf} represents the error due to deviation of atmospheric temperature from the assumed standard temperature profile. It can be shown that the error in indicated altitude due to a non standard temperature is of the form

$$e_{temp} = e_{hsf} \times h \tag{2-10}$$

so that the error due to non standard temperature is interpreted as an altimeter scale factor error. This error varies very slowly with time and location, such that it can be assumed to remain invariant over typical aircraft flight durations. The scale factor error is therefore modeled as a random constant

$$\dot{e}_{hsf} = 0 \tag{2-11}$$

with standard deviation σ_{hsf}.

The barometer's indication of altitude is based on static pressure (stationary aircraft). This static pressure must be inferred from pressure measurements made by a pitot-static tube aboard a moving aircraft. It can be shown assuming an exponential atmosphere that the altimeter error e_{sp} due to erroneous interference of the static pressure is approximately

$$e_{sp} = c_{sp} v^2 \tag{2-12}$$

where v is the aircraft speed. The coefficient c_{sp} is nearly invariant with altitude or density and is modeled as a random constant

$$\dot{c}_{sp} = 0 \tag{2-13}$$

with standard deviation σ_{sp}.

The barometric time delay represents the time required for the static pressure in the cavity of the pressure transducer to adjust to the static pressure at the port by flow of air through the tubing when the aircraft climbs or descends. This time constant is essentially invariant with time and is modeled as a random constant

$$\dot{\tau}_b = 0 \tag{2-14}$$

with standard deviation σ_{τ_b}.

At subsonic speeds and at low altitude, the standard setting error may be the most significant error. At subsonic speeds and at high altitude the scale factor error is usually the most significant error. At supersonic speeds, the static pressure measurement error may be the most significant. The altimeter lag is significant only during climbs and dives.

2.3 GPS Measurements Error Model

The GPS Space Segment will consist of 24 satellites in circular orbits having 12 hour periods and having inclinations of 63°. The satellites will be distributed in three orbital planes with each plane containing eight satellites at 45° intervals. The positions and velocities of these 24 satellites are included in the IGI Simulator [1].

Each satellite radiates a pseudo-random code signal, which is a known function of the GPS system time. The receiver in a GPS navigation set cross-correlates the received signal with a locally generated replica of the pseudo-random code signal to measure the received code time offset. This time offset measurement is called a pseudo-range measurement, because the measured time offset is a function not only of the range from the satellite to the receiver but also the receiver clock error relative to GPS system time.

In principle, pseudo-range measurements to four different satellites are sufficient for a navigation computer to solve for three components of vehicle position plus GPS system time. The accuracy of the solution is enhanced by choosing four satellites that provide favorable geometry. The satellite selection logic in the IGI simulator identifies the satellites that are in view above an elevation of 5°. For all combinations of four of these satellites, it computes the geometric dilution of precision. The set having the lowest dilution is selected for the next five-minute interval.

It is assumed that the Kalman filter processes a pseudo range difference measurement, which is the difference between the measured pseudo range and the range computed based on the given satellite ephemeris and on the INS indicated position. Such a difference measurement will be non-zero in the IGI simulator due to the simulated user clock phase error and due to the three components of INS indicated position error.

In addition to these sources of error which are states in the truth model, the pseudo range difference measurement is assumed to have an additive random error whose one-sigma

value is assumed to be 20 ft. This additive random error models other sources of GPS pseudo range measurement error including satellite clock compensation error, satellite ephemeris error, ionospheric retardation compensation error, tropospheric retardation compensation error, multipath random error, and receiver noise-related error. It is recognized that many of these sources of error are slowly varying, so in a future revision of the IGI simulator we shall introduce additional states in the truth model to represent the slowly varying external ranging errors. The omission of this model refinement in this present study is thought not to have a bearing on the principal results and conclusions.

A GPS receiver may also lock on to the suppressed carrier of the GPS signal. The offset between the received carrier frequency and the locally generated frequency is a function of the range-rate between the satellite and the receiver and of the user clock frequency error. Hence, this offset is called the pseudo range rate. The pseudo range rate is usually integrated to produce a delta-range measurement. When available, carrier tracking with the delta pseudo range measurement provides a more precise measure of the change in pseudo range than can be obtained by differencing successive pseudo-range measurements.

In the initial[1] and present version of the IGI Simulator, the delta pseudo range measurements are not simulated. In their place, pseudo range rate measurements are simulated. In a future version of the IGI Simulator, delta pseudo range measurements will be introduced.

It is assumed that the Kalman filter processes a pseudo range rate difference measurement, which is the difference between the measured pseudo range rate and the range rate computed based on the given satellite ephemeris and on the INS indicated velocity. Such a difference measurement will be non-zero in the IGI Simulator due to the simulated user clock frequency error states and due to the three components of INS indicated velocity error.

In addition to the sources of error which are states in the truth model, the pseudo range rate difference measurement is assumed to have an additive random error whose one-sigma value is assumed to be $1/\sqrt{5} = 0.45$ ft/sec. This error in a pseudo-range rate measurement is equivalent to an error in a delta-pseudo-range measurement of $\sqrt{5}$ ft 1σ with a 5 sec integration interval. A random error of $\sqrt{5}$ ft 1σ is

the result of the clock-phase white noise having spectral density of 1 ft^2/sec and integrating for 5 sec.

The initial[1,3] and present version of the IGI Simulator uses a four state clock error model (state variables 12, 13, 51, 52). A block diagram of the clock error equations is given in Figure 2-2.

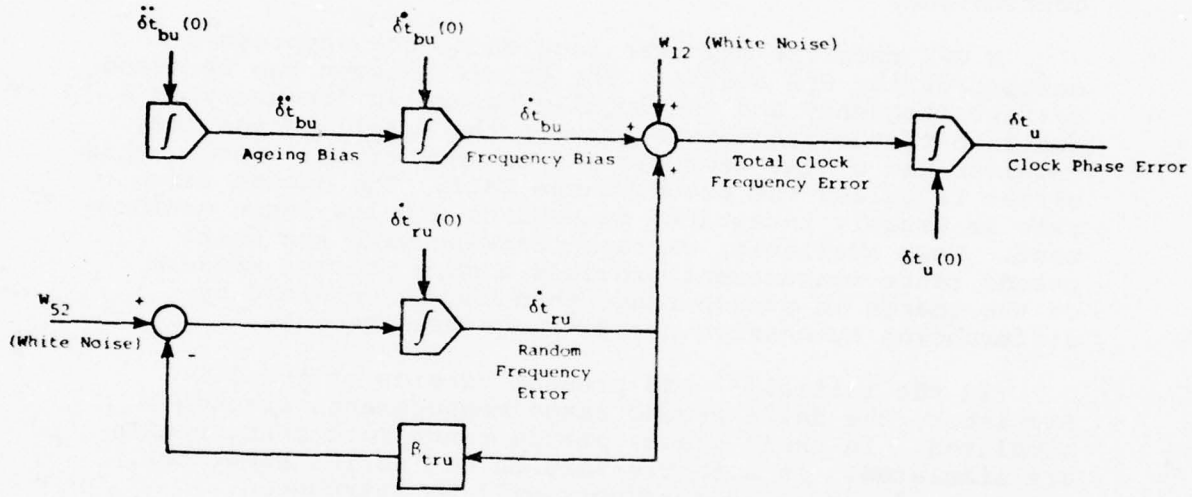

Figure 2-2 User Clock Error Model

Note in this model, the total clock frequency error is the sum of three terms: a white noise, a slowly shifting bias, and a first-order Markov error. Both the bias and Markov states are presently included as error sources in the pseudo-range rate measurements. The initial version[1] of the IGI Simulator did not include the effect of the Markov state frequency error in the simulated pseudo-range rate measurements. However, the one-sigma value of 10^{-6} ft/sec that was

assigned to the first-order Markov process was so small, that this omission may not have caused problems in the simulation results.

It is assumed that measurements are available every 5 sec. The measurement set includes eight measurements, which are the measured pseudo range and pseudo range rates to each of the four selected satellites. Periods of jamming are simulated by omitting the measurements for specified periods.

2.4 F4 Aircraft Trajectory

The precomputed reference trajectory which drives the error simulation model is representative of an F4 tactical mission profile. Figure 2-3 shows the ground track plot, while Figure 2-4 shows the altitude profile. In order to reduce the flight time simulated, only the high dynamics segment of the mission with appropriate lead in and lead out is used. This situation is reflected in the altitude profile of Figure 2-4. An examination of Figures 2-3 and 2-4 shows that between 300 and 400 secs, the aircraft executes a "figure eight" maneuver while losing altitude. Not evident in the ground track plot are the rapid zig-zag maneuvers executed by the aircraft. These are illustrated, however, by the yaw profile plot of Figure 2-5. In some of these maneuvers, maximum bank angles of 70° are used, with associated load factors of 3g. One pull-up has a load factor of 5g.

The mission scenario envisions a period of GPS signal jamming starting at T=685 secs just before the aircraft begins to descend towards a hypothetical target and ending at T=1110 secs as the aircraft is climbing away from the target. It is during this interval of jamming that differences can be expected in altitude and vertical velocity navigation accuracy of alternate vertical channel Kalman filter mechanizations.

2.5 Baro-Inertial Navigation Errors

In this subsection are exhibited the position and velocity errors of the simulated baro-inertial navigator as forced by the dynamics of the F4 aircraft trajectory.

In addition to the initial error source values and noise statistics presented in Table 2-5, initialization of the INS error model involves the selection and/or computation of appropriate initial values for INS position errors ($\delta\lambda$, δL, δh)

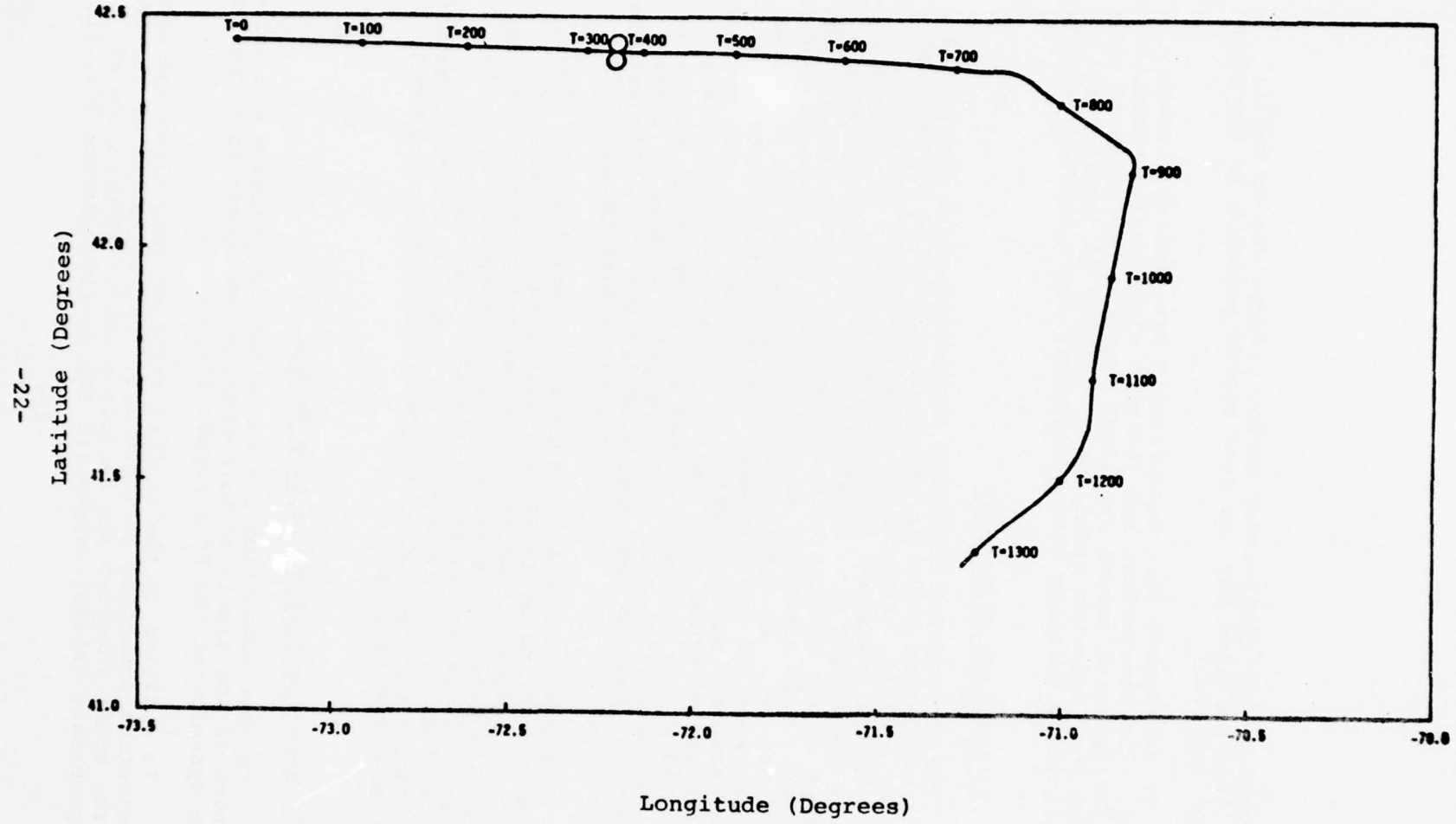

Figure 2-3 F-4 Mission Ground Track

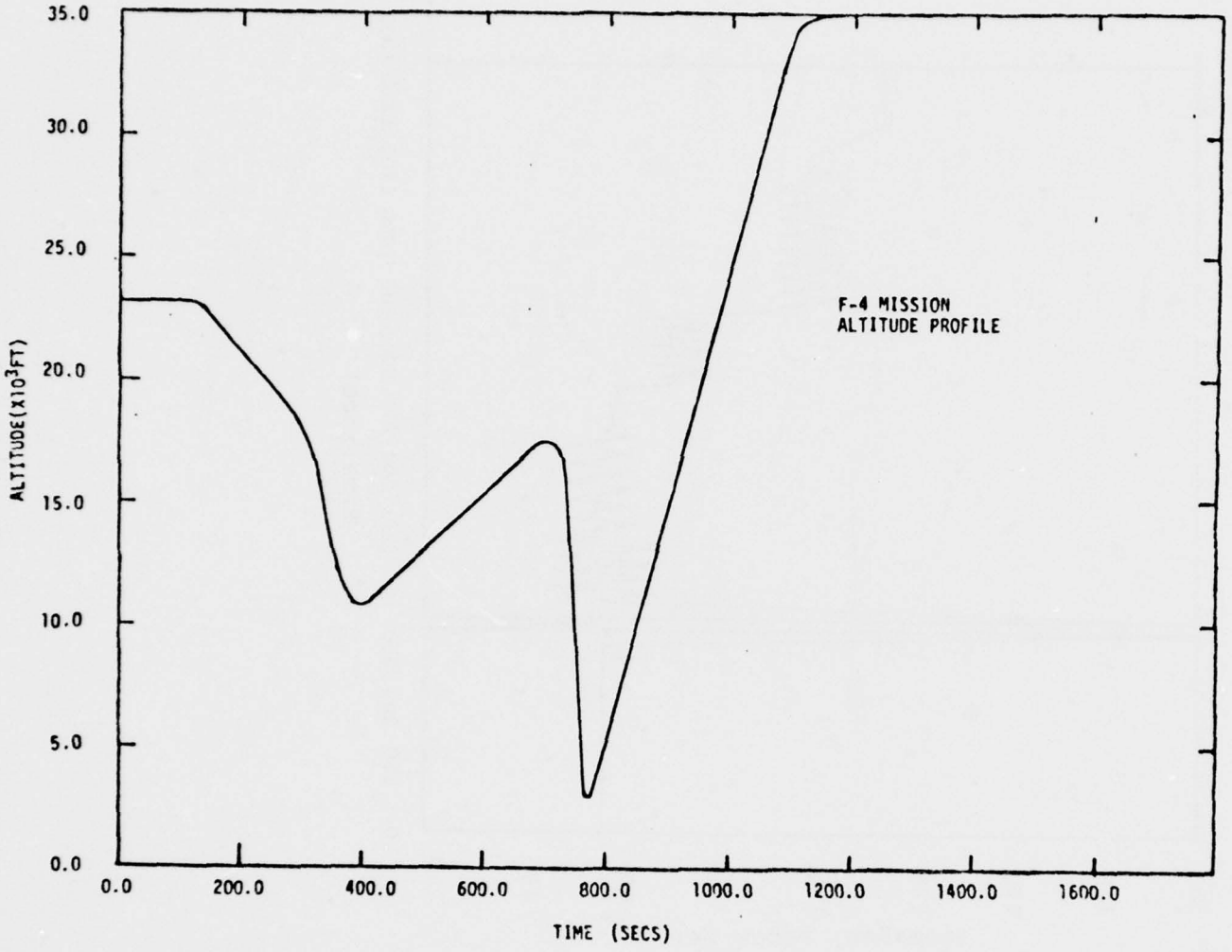

Figure 2-4 F-4 Mission Altitude Profile

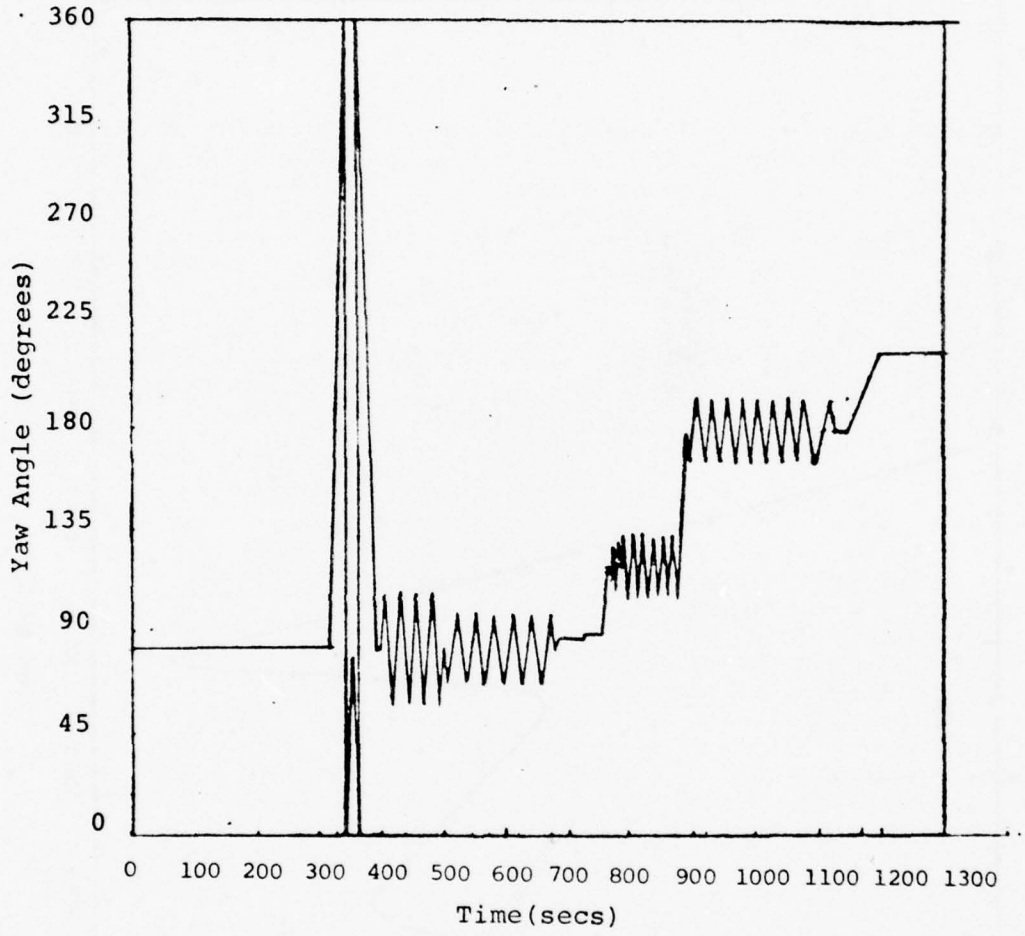

Figure 2-5 F-4 Mission Yaw Profile

velocity errors (δv_e, δv_n, δv_z), platform attitude errors (ε_e, ε_n, ε_z) and the vertical acceleration variable $\delta\hat{a}$.

At the start of the simulation, the aircraft is cruising at constant altitude. Representative and consistent initial values for the ten states mentioned above must be determined for this flight condition.

Initial values for the east and north attitude errors are assumed to correspond to 1 nautical mile of north and east position errors

$$\varepsilon_e(0) = -1 \text{ arc min}$$

$$\varepsilon_n(0) = +1 \text{ arc min}$$

The corresponding latitude error and longitude error are assumed to be:

$$\delta L(0) = -\varepsilon_e(0) \tag{2-15}$$

$$\delta\lambda(0) = \frac{\varepsilon_n(0)}{\cos L} \tag{2-16}$$

This correlation between horizontal position errors and horizontal components of attitude error is typical of Schuler oscillation inertial navigation errors.

In order to avoid a large transient in the vertical channel response, it is assumed that flight at constant attitude has been in progress sufficiently long so that the closed loop altitude error is equal to the baro-altimeter error. The initial value for the altitude error is therefore given by

$$\delta h(0) = e_{p_o}(0) + e_{hsf}(0) \times h(0) + c_{sp}(0) \times v^2(0) \tag{2-17}$$

using the initial values for e_{po}, e_{hsf}, and c_{sp} presented in Table 2-5, with h(0) = 23335 ft, v(0) = 819 ft/sec, then

$$\delta h(0) \approx 1300 \text{ ft}$$

Typical values of the velocity errors of a baro-stabilized inertial navigation system during cruise at constant altitude are of the order of 5 ft/sec for the east and north velocity errors and of the order of a tenth of a ft/sec for the vertical velocity error. Accordingly, the initial velocity errors have been chosen to be

$$\delta v_e(0) = 5.0 \text{ ft/sec}$$

$$\delta v_n(0) = 5.0 \text{ ft/sec}$$

$$\delta v_z(0) = 0.1 \text{ ft/sec}$$

In steady state the vertical acceleration error variable $\hat{\delta a}$ (state variable 11, which is the integral of the difference between the computed and barometric altitude) compensates for the inertial vertical acceleration error and permits the steady state difference between the computed altitude and barometric altitude to be zero. In the simulation runs conducted here, the initial value of $\hat{\delta a}$ compensates for vertical acceleration error due to vertical accelerometer bias, vertical accelerometer scale factor error, gravity anomaly, and gravity computation error, the initial value for $\hat{\delta a}$, is therefore given by

$$\hat{\delta a}(0) = AB_z(0) + ASF_z(0) \times g + \delta g_z(0) + \frac{2g}{R} \delta h(0) \qquad (2\text{-}18)$$

Using the initial values for AB_z, ASF_z and δg_z presented in Table 2-5, and $\delta h(0)$ as computed by Eq. (2-17), the appropriate initial value of $\hat{\delta a}(0)$ is

$$\hat{\delta a}(0) = 1.38 \times 10^{-2} \text{ ft/sec}^2$$

The data of Table 2-5 together with the relations and initial values for the basic position, velocity and attitude

error states, and for the variable $\hat{\delta a}$ presented above complete the INS error model initialization.

The resulting position and velocity errors of the baro-inertial system, unaided by GPS measurements, are shown in Figures 2-6, 2-7, and 2-8.

The horizontal position errors are shown in Figure 2-6. Both the one n.m. initial east and north position error show an initial upward trend due to the +5 ft/sec east and north velocity errors. Both plots display a segment of the familiar Schuler oscillation. The x (east) and y (north) accelerometer bias and effective misalignment errors (30 arc secs below the level plane) are the same, so that these sources of error have the same effect on east and north position errors. However, the ratio of east to north deflection of gravity is 1.53. This is also (approximately) the ratio of the changes from initial to peak value of the east and north position errors, which has a value of 1.49.

Figure 2-7 shows the INS horizontal velocity errors as functions of flight time. The downward trend together with the inflections of the plots at zero crossing points (where the respective position errors reach peak values) are associated with the Schuler oscillation. Between 300 and 400 seconds, the aircraft executes a right turn circle followed by a left turn circle as shown on the ground track plot of Figure 2-3. The fluctuation in the velocity errors during this interval are due to the misalignment errors of the x (east) and y (north) accelerometer about the vertical axis which cause the north and east components of acceleration during the turns to be misinterpreted respectively as having small components of east and north specific forces. The larger fluctuations in the east velocity errors are due to the larger effective misalignment of the x accelerometer from the east axis as shown in Figure 2-9. The subsequent zig-zag maneuvering of the aircraft shown in Figure 2-5 results in noticeable east velocity error fluctuations. The north velocity error fluctuations are much smaller because again the y accelerometer has a smaller misalignment and also because the east specific force is less than the north specific force when zig-zagging about an easterly heading. The yaw maneuvering between 900 and 1100 secs shown in Figure 2-5 results in much smaller east velocity error fluctuations because the aircraft is traveling southwards during this time.

Figure 2-8 shows the INS altitude and vertical velocity errors. The altitude error of the baro-inertial system sluggishly follows the total baro altimeter error which is dominated by the altimeter scale factor error and the

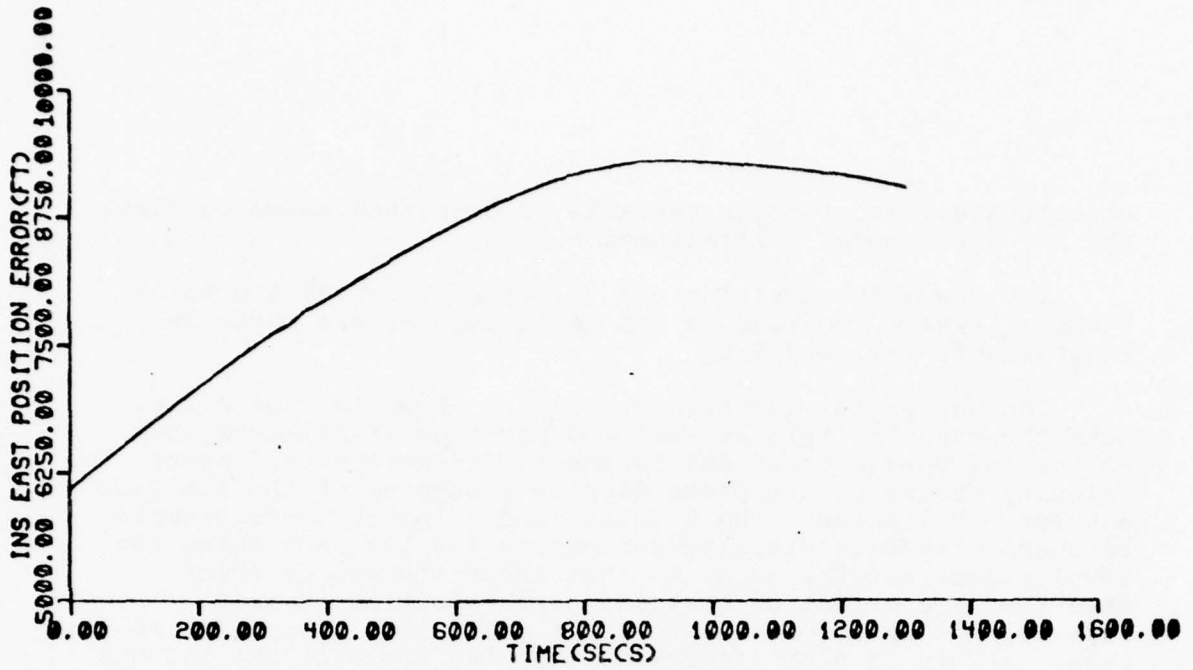

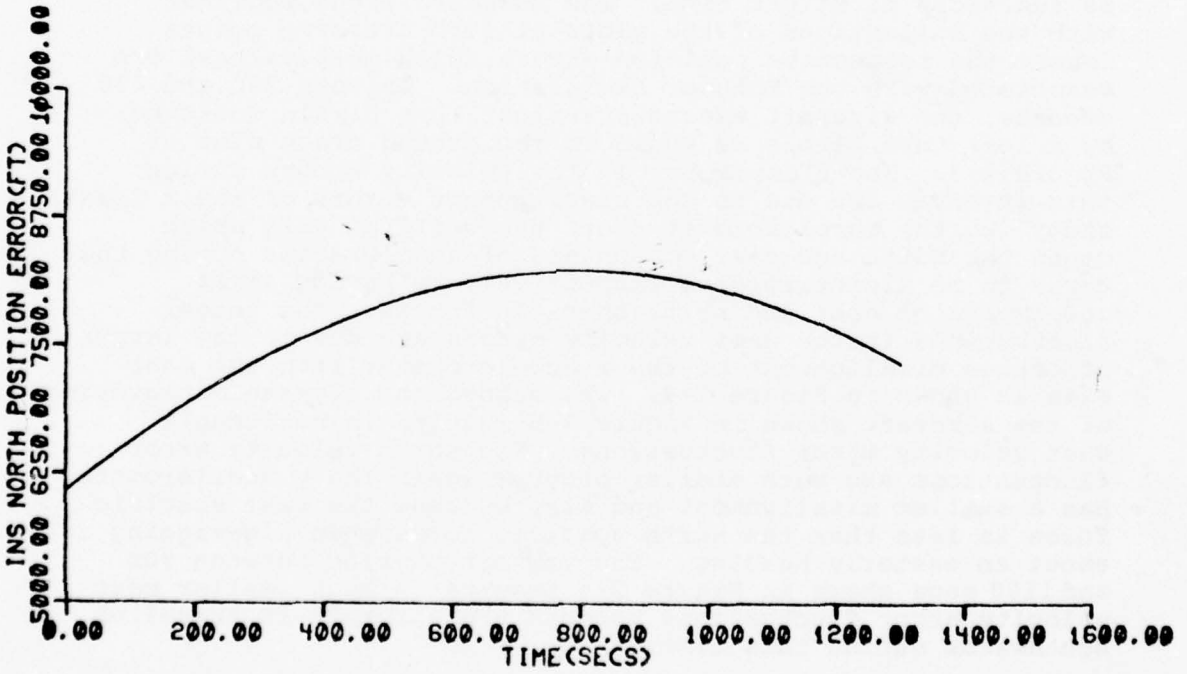

Figure 2-6 INS Horizontal Position Errors

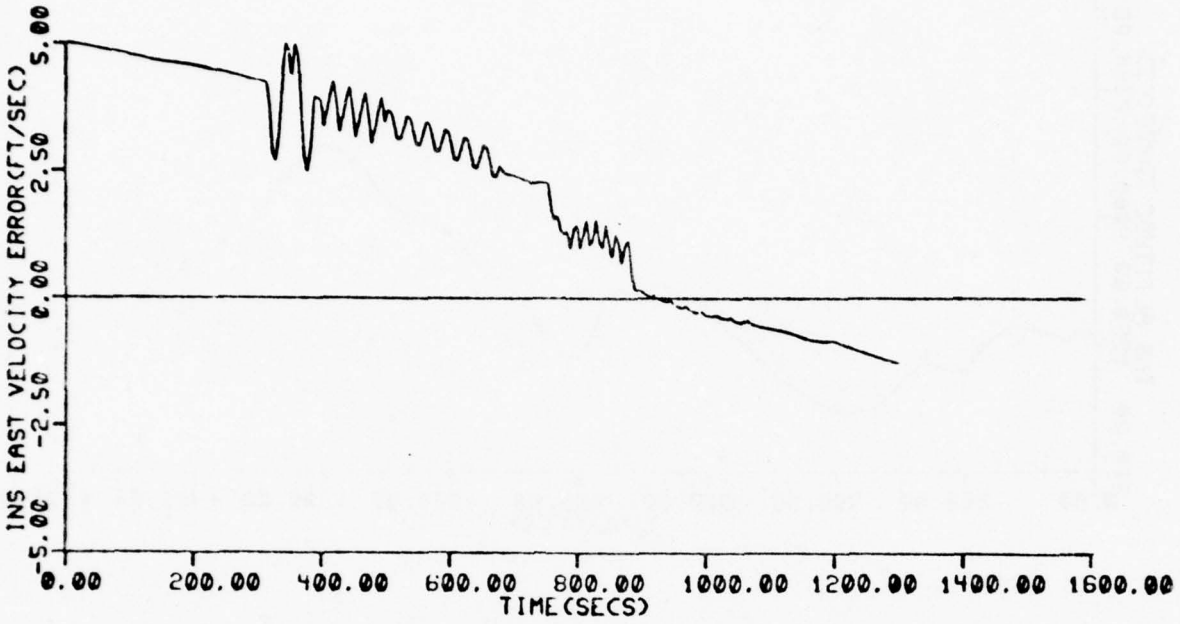

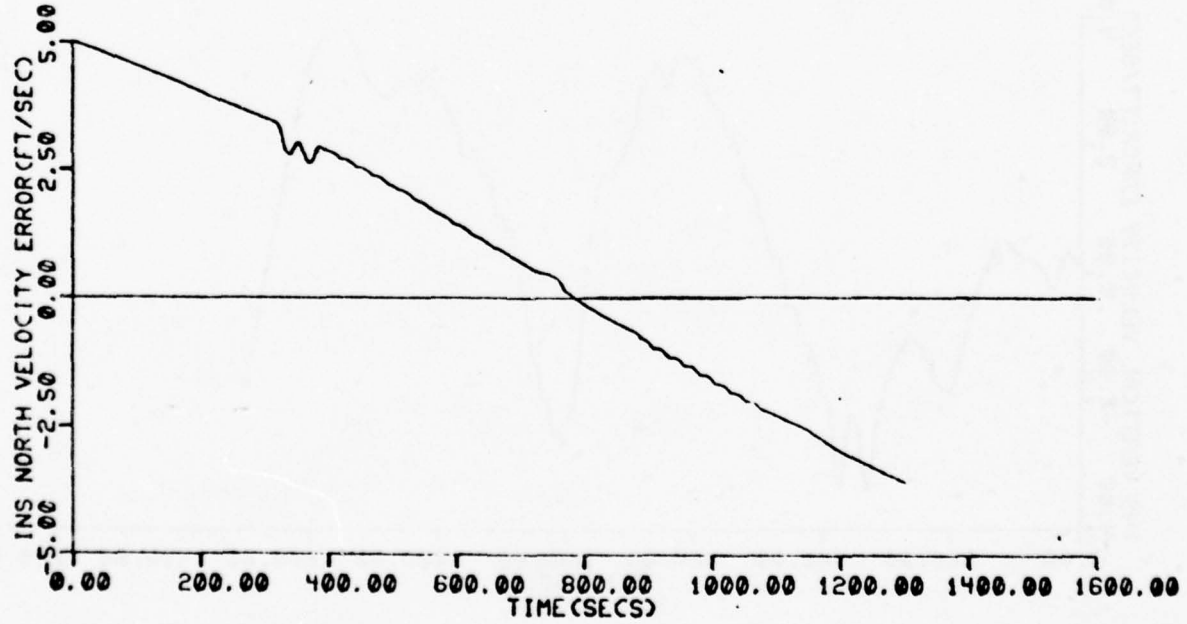

Figure 2-7 INS Horizontal Velocity Errors

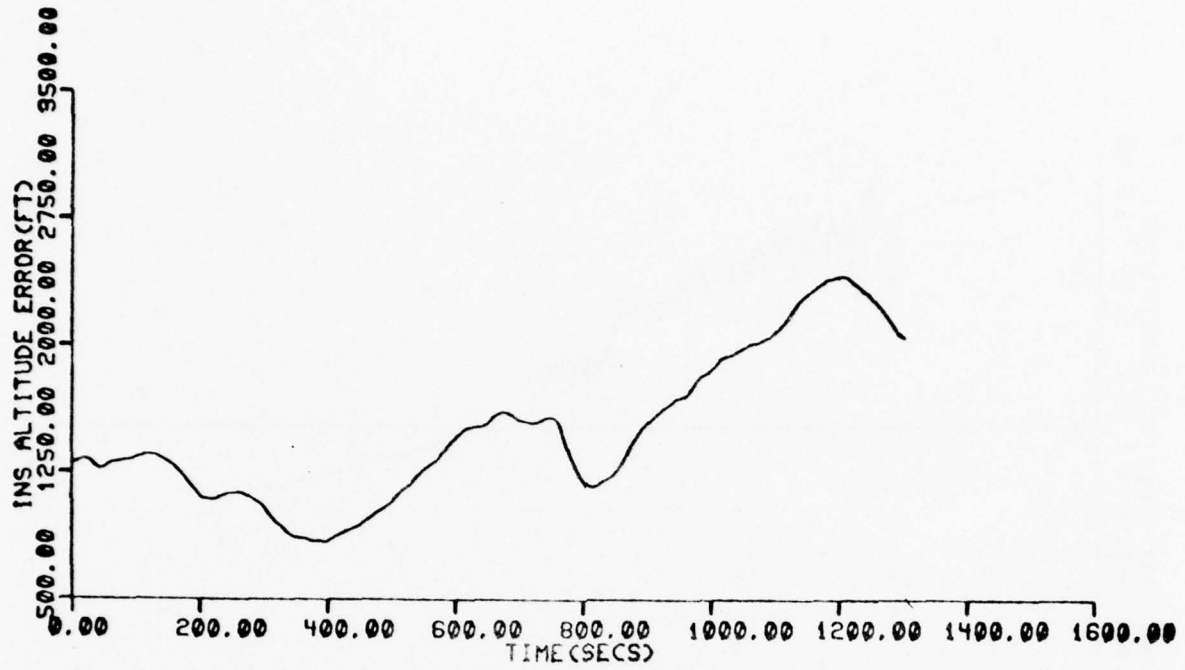

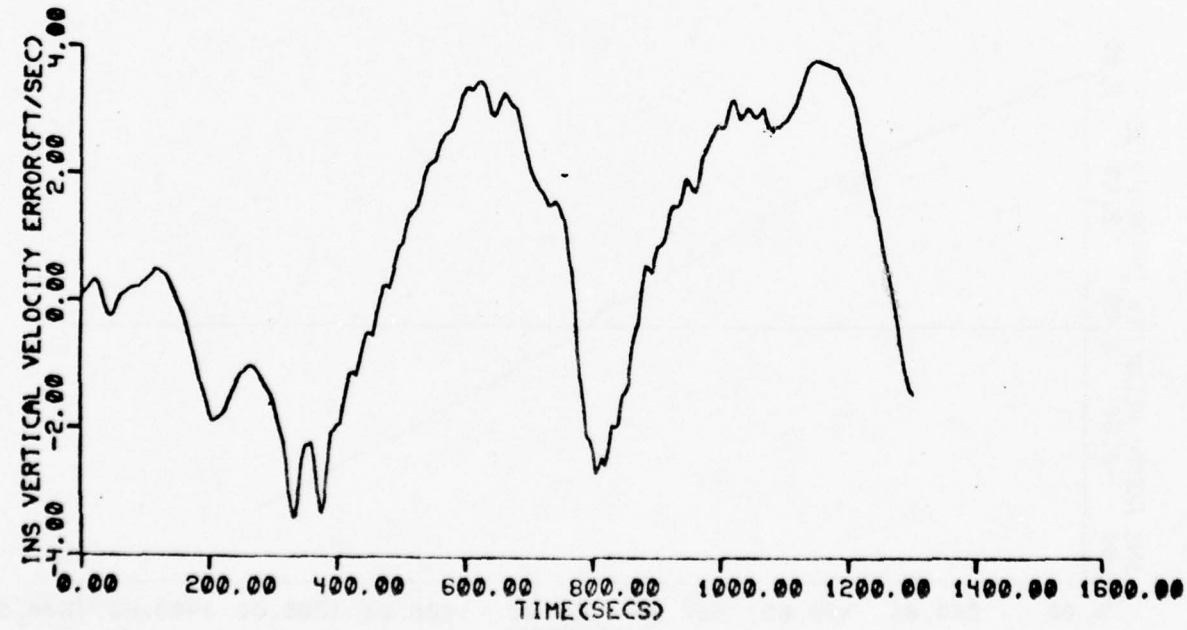

Figure 2-8 INS Altitude and Vertical Velocity Errors

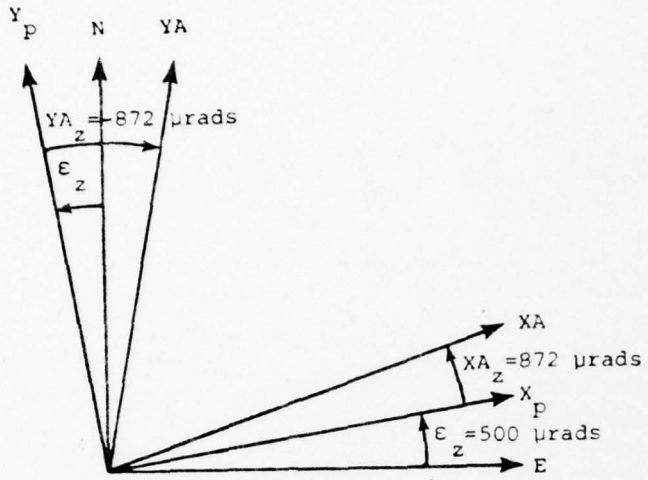

Figure 2-9 X and Y Accelerometer Misalignment from East and North

altimeter bias error. The latter error is modeled as a first order Markov process in the error model and assumes particularly severe values (up to 1150 ft) in this simulation run.

The low frequency content of the vertical velocity error is seen to follow sluggishly the rate-of-change of the altimeter error. High frequency variations in the vertical velocity error due to maneuver-dependent acceleration error are also evident in the figure.

SECTION III

FILTER ERROR MODELS

The IGI simulator currently mechanizes a Kalman filter for estimating navigation errors by processing GPS pseudo range and pseudo range rate measurements. The nominal trajectory about which the Kalman filter equations are linearized is that indicated by the unaided inertial navigation system, i.e., the INS indications of position and velocity.

In this section, three alternate filter mechanizations are discussed. These mechanizations differ in the manner in which the altimeter error is modeled. Section 3.1 first presents the basic filter state variables common to the three cases. Driving noises for these filter states are designed to account for sources of error not included as filter states. Section 3.2 discusses a two-state model for the altimeter error which includes an altimeter bias state and an altimeter scale factor error state. Section 3.3 discusses the single altimeter bias error state filter model for the altimeter error, while section 3.4 describes the single altimeter scale factor error state filter model. Section 3.4 discusses the models for the GPS measurements employed by the filter.

3.1 Inertial and Clock Error Models

The number of states selected for inclusion in the filter mechanization is a compromise between the requirements to obtain theoretically optimal performance and the requirements for filter implementation with reduced computation capacity. Table 3-1 presents the state variables to be estimated by the Kalman filter designs investigated here. Not defined in the table are the one or two states of the altimeter error model.

Table 3-1

Filter State Variables

STATE VARIABLE NUMBER	SYMBOL	DEFINITION	INITIAL FILTER STANDARD DEVIATION	
			VALUE	UNITS
1	$\delta\lambda$	Longitude Error	3.94×10^{-4}	Radians
2	δL	Latitude Error	2.905×10^{-4}	Radians
3	δh	Altitude Error	1500	Feet
4	δv_e	East Velocity Error	5	ft/sec
5	δv_n	North Velocity Error	5	ft/sec
6	δv_z	Vertical Velocity Error	1	ft/sec
7	ε_e	East Attitude Error	2.91×10^{-4}	Radians
8	ε_n	North Attitude Error	2.91×10^{-4}	Radians
9	ε_z	Azimuth Error	5.0×10^{-4}	Radians
10	δt_u	Clock Phase Error	1000	Feet
11	$\dot{\delta} t_{ru}$	Clock Frequency Error	10	ft/sec
12	Dx_f	X Gyro Drift	1.4554×10^{-8}	rads/sec
13	Dy_f	Y Gyro Drift	1.4554×10^{-8}	rads/sec
14	Dz_f	Z Gyro Drift	2.42×10^{-8}	rads/sec
15	δa_z	Filter Vertical Acceleration Error Variable	9.1793×10^{-3}	ft/sec^2
16	---	(Altimeter Error States to be Defined)	----	----
17	---		----	----

The first six states represent estimates of errors in the INS indications of vehicle position and velocity. The user's best estimate of position and velocity is obtained by subtracting the estimate of position and velocity error from the INS indications of these quantities. In other words, a positive position or velocity error estimate implies that the INS indication of position and velocity is greater (more positive) than the best estimate of position and velocity.

Positive values of the attitude error variables about a given axis implies that the platform is rotated positively (by the right hand rule) about that axis relative to the INS computed platform orientation with respect to the geographic frame.

The fundamental matrix of the error differential equations of the filter model for each of the three filters bears some correspondence to the upper left 16 x 16 partition of the truth model fundamental matrix. The basic 9 x 9 partition of Table 2-2a is also used in the three filters. The added elements of Table 2-2b are also utilized, but with appropriate changes to reflect the filter state numbering and the different filter altimeter error models. The gyro drift state coupling into attitude error in the filter is the same as the 3 x 3 lower left partition in Table 2-2c. The clock error model in the filter is similar to part of the truth error model of Table 2-2e as will be discussed later.

The omitted truth states which drive the position, velocity and attitude error differential equations are compensated for in the filter by assuming that the effects of the physical error sources that these states represent can be modeled as white process driving noises. The compensation equations presented below have been designed based on the methodology developed by Widnall in designing the CIRIS Kalman filter [4].

There are no omitted velocity error sources driving the position error dynamic equations, consequently, no compensating driving noises are added to the position equations.

The velocity errors are driven by several sources of acceleration error that are not included in the filter state vector. These acceleration errors are modeled as

white noises driving the velocity error states. The Kalman filter designer must assign values either to the elements of the noise vector spectral density matrix or to the elements of the resulting covariance matrix Q of the velocity error added during each filter cycle.

Specifying the noise covariance matrix is a most critical step in obtaining satisfactory filter performance. If elements in the assumed noise covariance matrix are too small, the filter will become overly optimistic about the accuracy of the extrapolated state estimate. This results in the underweighting of the current measurement data, and can lead to divergence of the estimated and actual state. If some elements in the assumed noise covariance matrix are too large relative to other elements, this causes an incorrect distribution of the measurement information to the various sources of error being estimated. The less-than-optimal distribution allows some errors to be badly estimated. For example, excessively large assumed noise covariance for the velocity error state variables can prevent satisfactory estimation of the platform misalignment.

It is common design practice to determine the driving noise covariance matrix by experiment, using simulation or real flight tests. The same (constant) matrix is used for each uniform time step. The driving-noise-covariance matrix for CIRIS as designed by Widnall[4] is a noticeable departure from this standard approach. The elements of the covariance matrix are computed as explicit functions of the assumed subsystem performance parameters and of the measured vehicle time-varying maneuvers.

The CIRIS methodology has been applied to the design of the driving noise covariance matrix for the IGI Kalman filter. In the case of the velocity error states, each filter cycle, the following east, north, and up variances are added to the respective diagonal elements of the velocity error covariance matrix:

$$Q_{ee} = \sigma_{max}^2\, 2v(\Delta v_e^2 + \Delta v_n^2)^{\frac{1}{2}} + (5 \times 10^{-5}\ \text{ft/sec})^2(\Delta t/.2\text{sec})$$

$$Q_{nn} = Q_{ee} \qquad (3\text{-}1)$$

$$Q_{zz} = Q_{ee}$$

where v is the vehicle speed, Δv_e and Δv_n are the integrated

east and north specific force during the time interval, and Δt is the time interval for which these increases apply. σ_{max} is the largest one sigma value from among the three accelerometer scale factor errors and the six accelerometer input axis misalignment angles. From the Table 2-5 data, the largest is seen to be 8.73×10^{-4} radians (180 arc sec).

Note in this simplified driving noise matrix, the east, north, and up variances are assumed equal and the off-diagonal covariances are assumed zero. A more accurate (and more complex) set of equations for the elements of the 3 x 3 noise covariance matrix may be found in the CIRIS design[4]. This more accurate set is an explicit function of the individual (different) one sigma values of the accelerometer scale factor errors and input axis misalignments, and it takes into account the specific orientation (wander angle) of the X and Y accelerometers relative to the east and north axes. These refinements were judged not necessary for this analysis.

The instrument-and-maneuver-dependent term in Eq.(3-1) has the property that if the vehicle is undergoing a 180° turn, the application of Eq.(3-1) each Kalman time interval will lead to a total added velocity error covariance in the filter that adequately matches the true added error covariance. The desired total result is also obtained in a prolonged longitudinal acceleration from slow speed to high speed (as in take-off), or the reverse.

During straight and level flight, when the horizontal components of specific force are zero, the maneuver dependent term in Eq.(3-1) is zero. It is desirable to have some minimum value of driving noise to model other sources of error such as shifts in the accelerometer bias and shifts in the gravity deflection. The second term in Eq.(3-1) serves this purpose. The numerical value selected is the same as that in the initial version of the IGI simulator, which added $(5 \times 10^{-5}$ ft/sec$)^2$ each 0.2 sec time update.

The attitude errors of the inertial system are driven by several sources of angular velocity error that are not included in the filter state vector. The most significant of these are normally the g-sensitive gyro drift rates. Again following the CIRIS design methodology, an appropriate covariance matrix for the effect of the

g-sensitive gyro drift rates in a maneuver has been selected. Each filter cycle the following east, north and up variances are added to the respective diagonal elements of the attitude error covariance matrix.

$$Q_{ee} = \sigma^2_{ASD} \quad 2v(\Delta v_e^{\,2} + \Delta v_n^{\,2})^{\frac{1}{2}} \qquad (3\text{-}2)$$

$$Q_{nn} = Q_{ee}$$

$$Q_{zz} = Q_{ee}$$

where σ_{ASD} is the one-sigma value of the uncompensated drift coefficients, which is the same for all six coefficients of the three IMU axes. Table 2-5 gives the value as being 0.3°/hr/g.

The filter model for the clock error includes only two states as shown in Fig. 3-1 below:

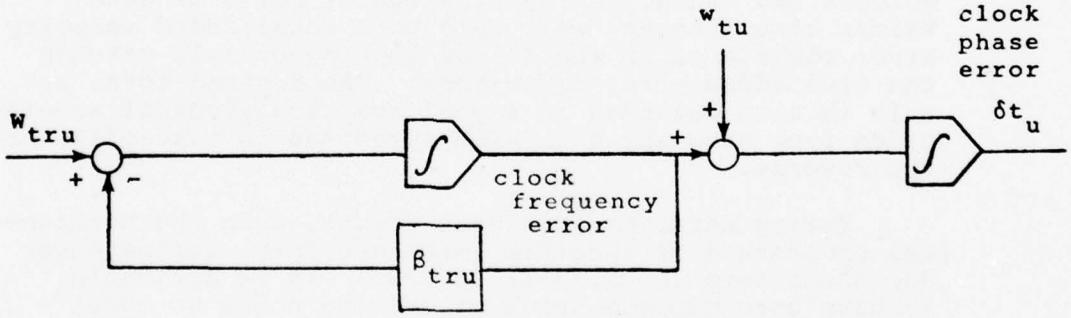

Fig. 3-1 Clock Error Model of the Filter

The clock phase error is modeled as having the same driving noise statistic used to drive the clock phase error state (state variable 10) in the truth model, namely, $N_{w_{tu}} = 1.0\ ft^2/sec.$

The clock frequency error is modeled as a first order Markov process with the same correlation time and driving noise statistic as that used in the truth model; i.e.,

$$N_{w_{tru}} = 2\beta_{tru}\,\sigma_{tru}^{2}\ \text{ft}^2/\text{sec}^3 \qquad (3\text{-}3)$$

The effects of error states 13 and 51 in the truth model are small, so are not included in the filter model.

The gyro drifts are modeled as random walks with the same driving noise statistics as those used in the truth model for the gyro drifts (states 14, 15, and 16):

$$N_{DXF} = (2.42 \times 10^{-10}\ \text{rads/sec})^2/\text{sec} = (.003°/\text{hr})^2/\text{hr}.$$

$$N_{DYF} = (2.42 \times 10^{-10}\ \text{rads/sec})^2/\text{sec} = (.003°/\text{hr})^2/\text{hr}.$$

$$N_{DZF} = (4.03 \times 10^{-10}\ \text{rads/sec})^2/\text{sec} = (.005°/\text{hr})^2/\text{hr}.$$

The filter vertical acceleration error state variable δa_z is defined to be:

$$\delta a_z = \hat{\delta a} - \overline{\delta a} \qquad (3\text{-}4)$$

where $\hat{\delta a}$ is the LN-15 computed estimate of the vertical acceleration error (state 11 of the truth model) and $\overline{\delta a}$ is the slowly varying part of the error in the vertical acceleration and that is not modeled as state related. Some various sources of acceleration error δa were given in Eq.(2-5). The terms in Eq.(2-5) modeling the normal gravity computation error and the acceleration error due to platform attitude error are filter-state related (δh, ε_e, ε_n) and are modeled properly in the filter fundamental matrix. The acceleration error due to accelerometer input axis misalignment is not slowly varying (the horizontal specific force usually varies rapidly compared with the vertical channel time constant). This leaves the following terms as included in $\overline{\delta a}$:

$$\overline{\delta a} = AB_z + gASF_z + \delta g_z \qquad (3\text{-}5)$$

where AB_z is the accelerometer bias, ASF_z is the accelerometer scale factor, and δg_z is the gravity anomaly. To obtain the elements of the filter fundamental matrix associated with the δa_z row, one may differentiate the definition (3-4), using Eq.(3-5). It can be shown that the derivative is:

$$\dot{\delta a}_z = k_3(\delta h - \delta h_b) - w_{ABz} \qquad (3\text{-}6)$$

The first term (with the vertical channel gain k_3) is related to the filter state δh and the filter states that are chosen to model the altimeter error. The second term is the white noise associated with the accelerometer bias random walk model. In differentiating the terms in Eq.(3-5) we have assumed $gASF_z$ is constant and we have neglected the rate of change of the gravity anomaly. The appropriate expression for the growth Q_{az} in the variance of the vertical acceleration state due to the white noise and to be used each filter time update is:

$$Q_{az} = N_{ABz}\,\Delta t \qquad (3\text{-}7)$$

The filter uses a value for the noise spectral density of $(10\ \mu g)^2/hr.$, which is the same as is assumed in the truth model.

3.2 Two-State Altimeter Error Model

Filter A has two states representing the altimeter sources of error: One state a bias error and the other state a scale factor error:

$$\delta h_b = e_{po} + e_{hsf}\,h \qquad (3\text{-}8)$$

where:

e_{po} = Altimeter bias error state

e_{hsf} = Altimeter scale factor error state

h = Aircraft altitude

As in the truth model, the altimeter bias error is modeled as a first order Markov process:

$$\dot{e}_{po} = -\omega_{alt}\, e_{po} + w_{epo} \qquad (3\text{-}9)$$

$$\omega_{alt} = v/d_{alt} \qquad (3\text{-}10)$$

$$N_{epo} = 2\omega_{alt}\, \sigma_{alt}^{2} \qquad (3\text{-}11)$$

where:

d_{alt} = Correlation distance of the weather patterns

σ_{alt} = Standard deviation of altimeter bias

N_{epo} = Spectral density of white noise w_{epo}

Numerical values for d_{alt} and σ_{alt} are the same as those used in the truth model; i.e.,

d_{alt} = 250 n.m.

σ_{alt} = 500 ft.

The altimeter scale factor error is similarly modeled as a first order Markov process but with a fixed correlation time of two hours:

$$\dot{e}_{hsf} = -\beta_{e_{hsf}}\, e_{hsf} + w_{e_{hsf}} \qquad (3\text{-}12)$$

where:

$$\beta_{e_{hsf}} = \frac{1}{7200\,(\text{sec})}$$

The spectral density of the white noise we_{hsf} is related to the standard deviation of the scale factor error by:

$$N_{e_{hsf}} = 2\beta_{e_{hsf}} \sigma_{e_{hsf}}^{2} \qquad (3\text{-}13)$$

The standard deviation σ_{ehsf} used in equation (3-13) is the same as that used in the truth model; i.e.,

$$\sigma_{hsf} = 0.03$$

Note that even though the truth model treats the scale factor error as a random constant, we have used a first order Markov model in the filter. This ensures that the filter gains associated with estimating the altimeter scale factor will not go to zero.

3.3 Bias Single State Altimeter Error Model

In filter B, the altimeter error δh_b is modeled by a single bias-like state e_{bh}:

$$\delta h_b = e_{bh} \qquad (3\text{-}14)$$

A random walk model is adopted for this state:

$$\dot{e}_{bh} = w_{e_{bh}} \qquad (3\text{-}15)$$

This altimeter model is the same as that used in the CIRIS filter[4]. It is shown that a suitable expression for the altitude error variance growth during each filter cycle is:

$$Q_{e_{bh}} = 2(v/d_{alt})\, \sigma_{alt}^{2}\, \Delta t + \sigma_{e_{hsf}}^{2}\, 2h\, |\Delta h| \qquad (3\text{-}16)$$

This noise variance includes a term associated with the variation in the bias due to the variation in the height

of a constant pressure surface and a term which models the shift in the bias due to the scale factor error and a change in altitude. It can be shown that in a climb from near sea-level to the final altitude h_f, the repeated application of Eq.(3-16) each filter time update leads to a total added altimeter error variance from the second term of $(\sigma_{e_{hsf}} h_f)^2$, which is exactly the error variance at altitude due to scale factor error.

Not included in Eq.(3-16) is an additional term from the CIRIS design which can model the shifts in altimeter bias due to speed changes and the static pressure measurement error. At subsonic speeds, modeling this effect in the filter is not necessary.

3.4 Scale Factor Single State Altimeter Error Model

In filter C, the altimeter error δh_b is modeled by a single effective scale factor error state e_{seff}:

$$\delta h_b = h\, e_{seff} \qquad (3\text{-}17)$$

Assuming the two most significant sources of error are the true scale factor error e_{hsf} and the bias e_{po} due to the zero-setting error, then the effective scale factor error in terms of the two sources is:

$$e_{seff} = e_{hsf} + e_{po} / h \qquad (3\text{-}18)$$

A random walk model is adopted for this state:

$$\dot{e}_{seff} = w_{eseff} \qquad (3\text{-}19)$$

The Kalman filter needs an expression for the spectral density N_{eseff} of the assumed white noise, or equivalently for the growth Q_{eseff} in the variance of the estimate of the effective scale factor error in a filter time step Δt. Consider the differential of Eq.(3-18):

$$\Delta e_{seff} = \Delta e_{hsf} + (\Delta e_{po})/h + e_{po}\, \Delta(1/h) \qquad (3\text{-}20)$$

This differential suggests that the changes in the effective scale factor error may be considered to arise in three ways: from changes in the true scale factor error, from changes in the zero setting error, and from changes in altitude in the presence of a non-zero zero-setting error. The mean value of the differential is zero, because the mean of each term is zero. The mean square value of the differential is the sum of the mean square values of each term, because each term is statistically independent. This suggests an expression for the growth Q_{eseff} in the variance of the estimate of the effective scale factor error be made up of the sum of three terms:

$$Q_{eseff} = Q_{ehsf} + Q_{epo} / h^2 + \sigma_{alt}^2 [\Delta(1/h)]^2 \quad (3\text{-}21)$$

The first term can utilize the noise spectral density from Eq.(3-13), which accounts for the random walk nature of the true scale factor error:

$$Q_{ehsf} = 2\beta_{ehsf} \sigma_{ehsf}^2 \Delta t \quad (3\text{-}22)$$

The second term can utilize the noise spectral density from Eqs.(3-11) and (3-10), which accounts for the random walk nature of the zero-setting error:

$$Q_{epo} = 2(v/d_{alt}) \sigma_{alt}^2 \Delta t \quad (3\text{-}23)$$

The third term requires some discussion. In line with the CIRIS design methodology, we seek an alternate expression for the third term which is a function of the current altitude h and the change Δh in altitude during the current filter time step. It can be shown that an upper bound on the square of the change in inverse altitude is:

$$[\Delta(1/h)]^2 = (1/h_1 - 1/h_2)^2 < 1/h_1^2 - 1/h_2^2 \quad (3\text{-}24)$$

$$\text{for } 0 < h_1 < h_2$$

Note this bound is a definite integral:

$$\int_{h_1}^{h_2} 2(1/h^3)\, dh = 1/h_1^2 - 1/h_2^2 \qquad (3\text{-}25)$$

$$\text{for } 0 < h_1 < h_2$$

This suggests an appropriate alternate expression for the third term as being:

$$Q_{\Delta h} = \sigma_{alt}^2 2(1/h^3)\ |\Delta h| \qquad (3\text{-}26)$$

Repeated application of this expression, each Kalman time update, leads to a total added variance which is an upper bound on the added variance due to the complete climb or descent.

Using Eqs.(3-22), (3-23), and (3-26), the expression used in filter C for the growth in the variance of the effective scale factor error estimate is:

$$Q_{eseff} = 2\beta_{ehsf}\, \sigma_{ehsf}^2\, \Delta t + 2(v/d_{alt})\, \sigma_{alt}^2\, \Delta t/h^2 + \sigma_{alt}^2\, 2(1/h^3)\ |\Delta h| \qquad (3\text{-}27)$$

Note the fundamental difference between the above effective scale factor error model and the scale factor error model evaluated by Myers and Butler[1,3]. The above model is a random walk model, whereas the Myers/Butler filter model used a random constant model. The random walk model ensures that the Kalman gain associated with estimating the effective scale factor error will not go to zero.

3.5 Measurements Error Model

The truth model for the errors in the GPS measurements were discussed in Section 2.3. The Kalman filter processes a pseudo range difference measurement and a pseudo range-rate difference measurement. These measurements are the

differences between the receiver-measured quantities (pseudo range and pseudo range-rate) and the computed quantities based on the INS indicated position and velocity and on the satellite ephemeris.

The Kalman filter employs linearized models for these difference measurements:

$$z_{pr} = \underline{h}_{pr}^{T} \underline{x} + v_{pr} \qquad (3\text{-}28)$$

$$z_{\dot{p}r} = \underline{h}_{\dot{p}r}^{T} \underline{x} + v_{\dot{p}r} \qquad (3\text{-}29)$$

where $\underline{h}_{pr}$ and $\underline{h}_{\dot{p}r}$ are the measurement gradient vectors, $\underline{x}$ is the filter state vector and v_{pr} and $v_{\dot{p}r}$ are additive random error. Non-zero elements in the pseudo range difference gradient vector are associated with the position error states and the clock phase error state. Non-zero elements in the pseudo-range-rate difference gradient vector are associated with the velocity error states and with the clock frequency error state.

Values assumed in the filter for the variances of the additive random errors are the same as for the actual errors in the truth model, namely:

$$\sigma_{pr} = 20 \text{ feet}$$

$$\sigma_{\dot{p}r} = 0.45 \text{ ft/sec}$$

SECTION IV

INTEGRATED GPS/INERTIAL PERFORMANCE

The IGI Simulator has been used to evaluate the three alternate Kalman filter vertical channel designs, which were developed in the previous section. Each filter was exercised using the same truth model for the sources of error and using the same F4 aircraft trajectory. The truth model and trajectory were presented in Section 2. This section presents and discusses the simulation results.

The results are presented in terms of plots, which contain both the estimation error and the filter-computed uncertainty. The estimation error is the difference between the Kalman filter best estimate of a variable and the true value of a variable as known from the truth model. The filter-computed uncertainty or one-sigma value is the square root of the appropriate diagonal element of the filter estimation error covariance matrix. This one-sigma value has been plotted both plus and minus to establish a visual band for evaluating the filter performance. For both the errors and the uncertainties, plot points include the values both before and after incorporating each set of eight pseudo range and pseudo range-rate measurements.

In the presentations which follow, Case A uses the filter with the two-state altimeter error model, Case B uses the filter with the random walk bias single-state altimeter error model, and Case C uses the filter with the random walk effective scale factor single-state altimeter error model.

A comparison of the horizontal position and velocity errors is presented first in Subsection 4.1, followed by a comparison of the vertical channel errors in Subsection 4.2. The attitude errors are discussed in Subsection 4.3. The clock phase and frequency errors are discussed in Subsection 4.4.

4.1 Horizontal Position and Velocity Errors

The horizontal position and velocity errors of the three cases are compared in Figures 4-1 through 4-4. There is little difference between the three cases. A reasonable conclusion is that the differences in the three vertical channel designs produce only second order effects. in the horizontal position and velocity.

During the initial flight segment with full GPS availability, the filter-computed east and north position uncertainties are about ten to twelve feet. During the simulated jamming period between 685 sec and 1110 sec, during which no GPS measurements were available, the estimation errors and the computed uncertainties grow significantly. A "flat top" corresponds to an off-scale value of a variable. The east position error in Figure 4-1 is generally within the filter-computed uncertainty.

The north position error shown in Figure 4-2 has a bias of about twenty feet. We believe this bias is a result of the choice of the reference position about which the Kalman filter measurement processing equations are linearized. In both the original version of the IGI Simulator[1] and in the present version used in this study, the Kalman filter processes a pseudo range difference measurement z that is the difference between the receiver-measured pseudo range and the computed pseudo range based on the INS indicated position. The filter forms its own a priori best estimate $\hat{z}$ of the measurement using a linearized model for the relationship between the best estimate of the state x and the measurement:

$$\hat{z} = \underline{h}^T \underline{x}^- \qquad (4\text{-}1)$$

The filter then uses the residual difference between the measurement and the expected measurement to update the state vector:

$$\underline{x}^+ = \underline{x}^- + \underline{k}(z - \hat{z}) \qquad (4\text{-}2)$$

In the present study, the simulated INS east and north position errors are both of the order of 7,000 feet, as was shown in Figure 2-6. The filter rapidly converges to estimages of the position errors that are close to the true errors. Hence the INS latitude and longitude error elements in the filter state vector are angles representing

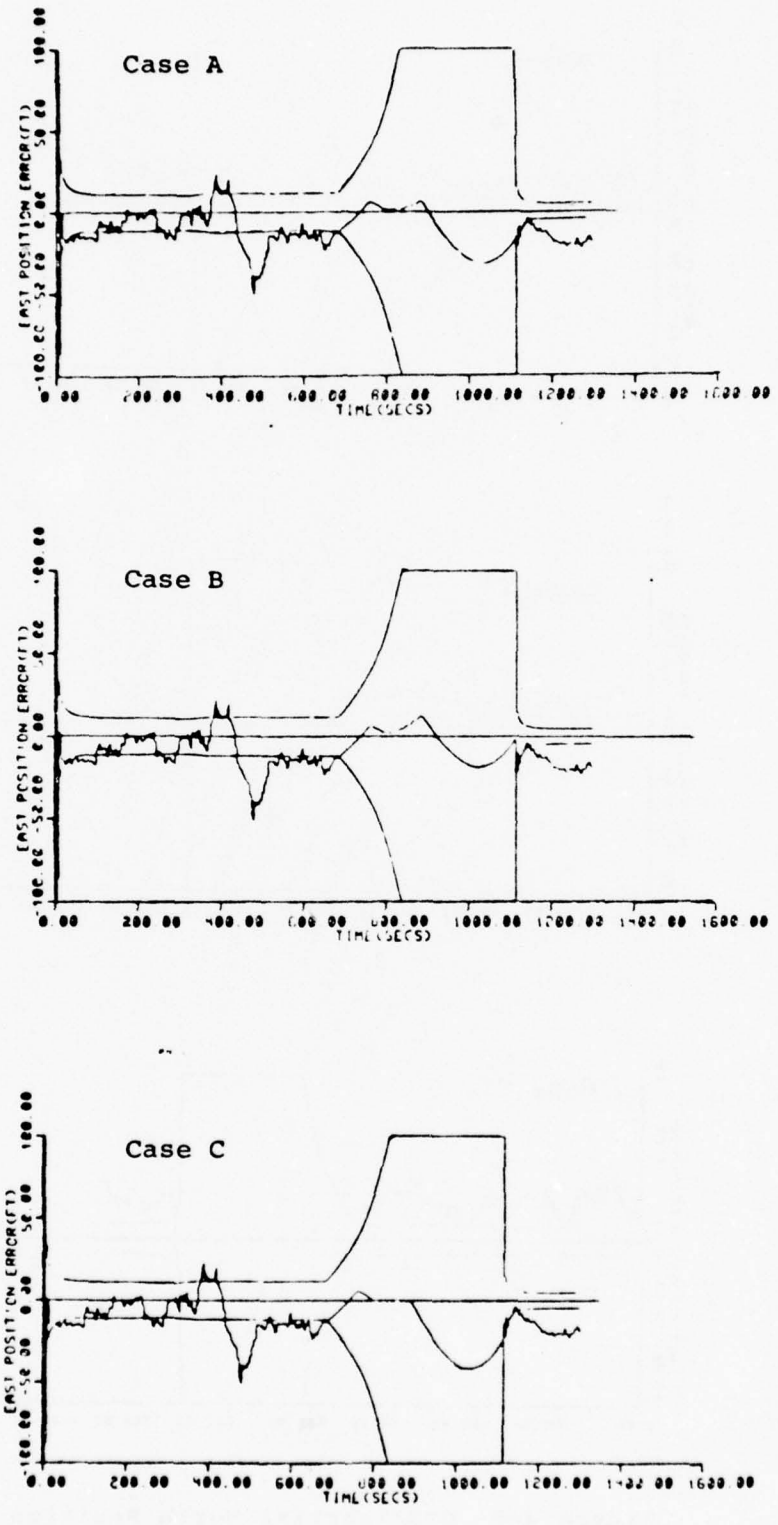

Figure 4-1 GPS/Inertial East Position Errors

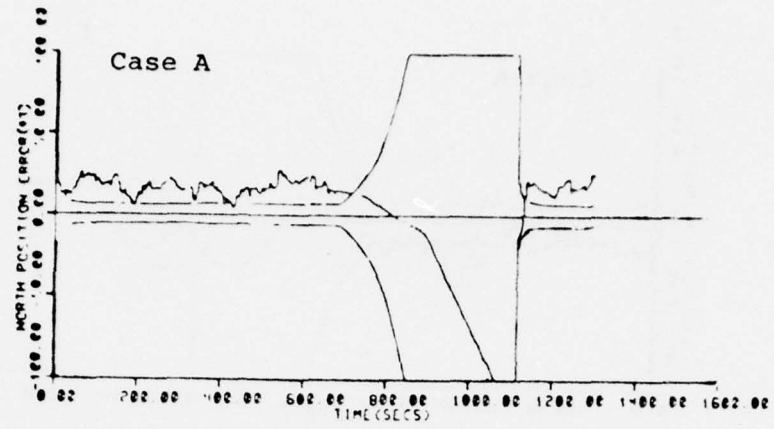

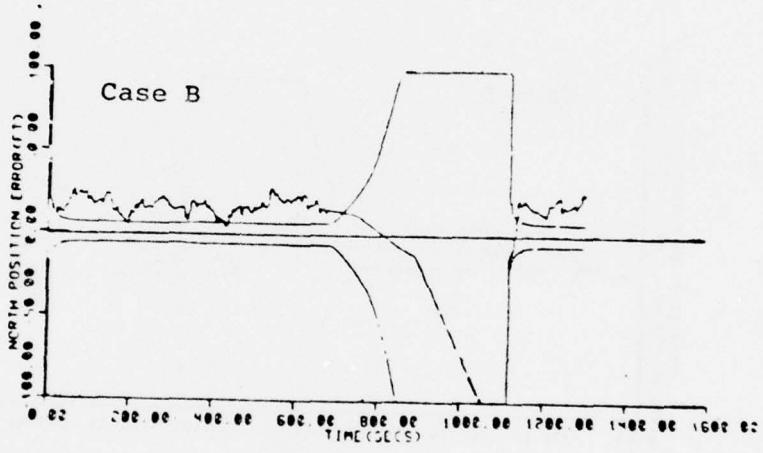

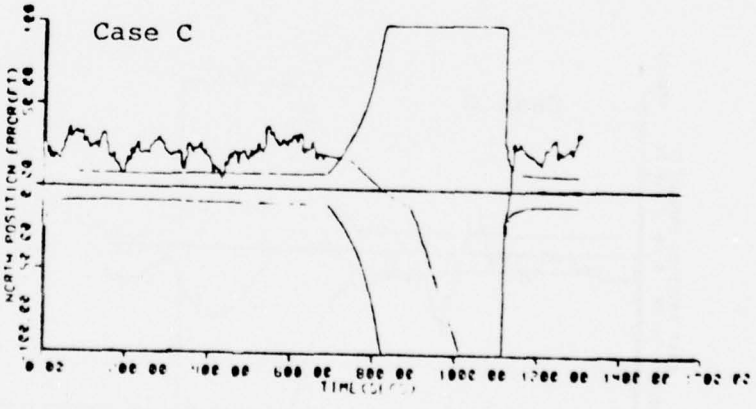

Figure 4-2 GPS/Inertial North Position Errors

the order of 7,000 feet. The measurement gradient vector $\underline{h}$ was derived using a spherical earth assumption. As a result, the elements of $\underline{h}$, which give the rate of change of the difference measurement with respect to longitude error and latitude error, are functions of a value of earth radius that is not precisely equal to the local earth radius of curvature. The value is wrong by about 0.3% compared with the correct curvature for the latitude element. This 0.3% error in the latitude error element of $\underline{h}$ when multiplying a latitude error state estimate of 7,000 feet leads to an error in the best estimate of the pseudo range difference of about twenty feet (for satellites in a northerly or southerly direction). The Kalman filter must converge to an estimate of the state that leaves no bias in the residual. It does this by having a 0.3% error (twenty feet) in its best estimate of INS latitude error to offset the 0.3% error in $\underline{h}$. The value for earth curvature used for the longitude error state happens to be more nearly correct, so a similar large bias in east position error is not produced.

This biasing effect can be eliminated either by using more accurate expressions for the elements of the $\underline{h}$ vector or by changing the reference position about which the measurement processing equations are linearized. One form of the second approach is to utilize a pseudo range difference measurement that is the difference between the receiver-measured pseudo range and the computed pseudo range based on the filter best estimate of position. An equation like Eq.(4-1) is then not needed (except perhaps for the clock phase error) because the best estimate of the difference measurement is zero.

The horizontal velocity errors are shown in Figures 4-3 and 4-4. The east and north results are similar. During the first 300 sec (before any turns), the velocity errors are about 0.2 ft/sec. At about 300 sec the rapid maneuvering begins. The filter-computed uncertainties increase due to the maneuver-dependent noise covariance. East velocity error peaks larger than one ft/sec are seen. The error fluctuations are similar in amplitude to the INS (no GPS) east velocity error shown in Figure 2-7. During the period of jamming, the velocity errors stay under one ft/sec. The INS velocity errors in this period are shifting more than two ft/sec. The filter computed uncertainty in this period is somewhat conservative.

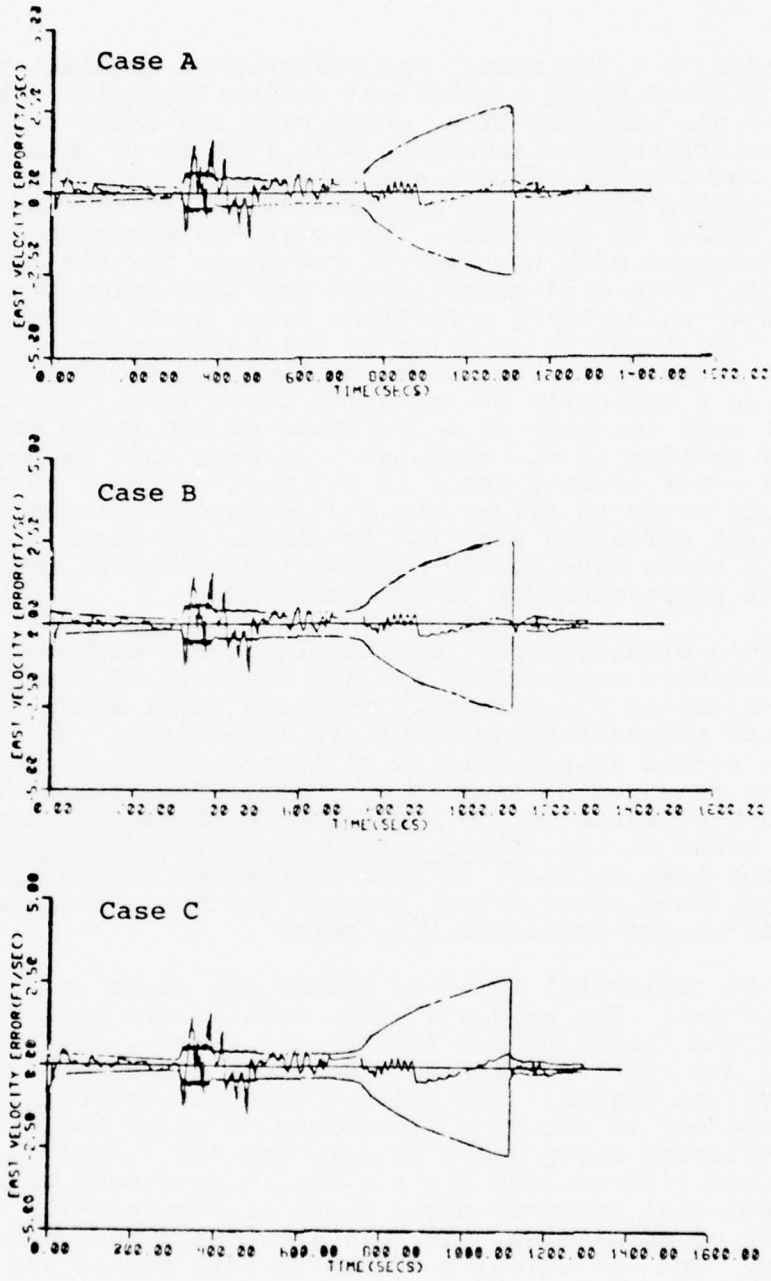

Figure 4-3 GPS/Inertial East Velocity Errors

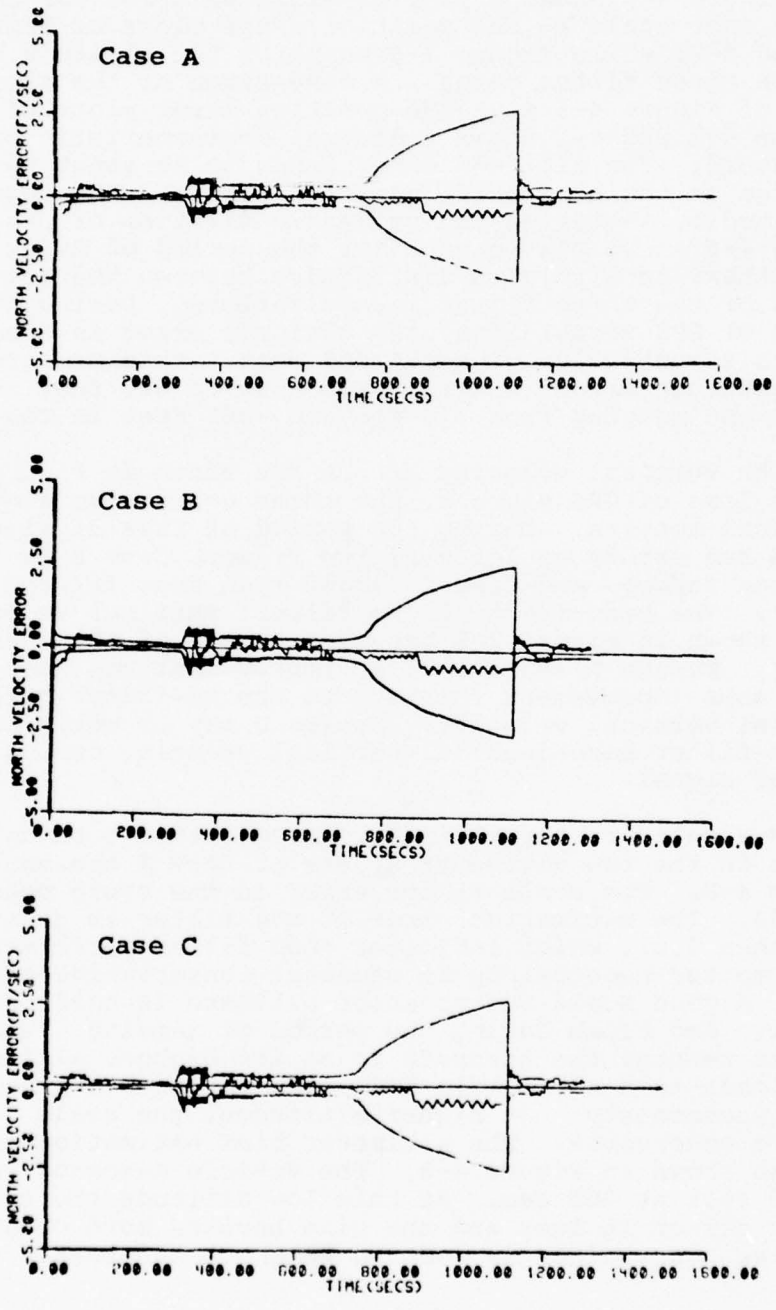

Figure 4-4 GPS/Inertial North Velocity Errors

4.2 Vertical Channel Errors

Figure 4-5 shows a plot of altitude error for Case A on the same scale as the position error plots of Figures 4-1 and 4-2, while Figure 4-6 compares the altitude errors for the three filter cases. A comparison of the altitude error of Figure 4-5 with the position error plots of Figures 4-1 and 4-2 shows a general characteristic of GPS navigators: The altitude error tends to be about twice as large as the horizontal position errors. This can be explained by analyzing the geometric dilution of precision. Figure 4-6 shows that except for the period of GPS signal loss, there is little to distinguish between the altitude errors of the three filter mechanizations. During the period of GPS signal loss, the altitude error in Case A reaches a peak value of about 400 feet. This compares with altitude errors ranging from -340 to 680 feet in Case B and ranging from 770 feet to -885 feet in Case C.

The vertical velocity errors are shown in Figure 4-7. Before loss of GPS signals, the three cases give almost identical results. During the period of loss of signal, Case A has errors as large as two ft/sec, Case B as large as three ft/sec, and Case C larger than four ft/sec (off scale). The baro-inertial (no filter) vertical velocity error shown in Figure 2-8 has peak errors of three and four ft/sec. Design A shows a clear improvement and design B shows some improvement relative to the no-filter baro-inertial vertical velocity. Design C may be worse than the no-filter baro-inertial vertical velocity during the loss of signal.

How well are the altimeter error states working? The errors in the two altimeter states of Case A are shown in Figure 4-8. The scale factor error in the truth model is 0.03. The estimation error of the filter is generally less than 0.01, which indicates good filter performance. The computed uncertainty is somewhat conservative being at 0.02. A good scale factor error estimate is held through the dive and climb during the period of jamming. When GPS signals return, the aircraft is at its highest altitude. This leads to a noticeable reduction in the scale factor error uncertainty. At higher altitudes, the scale factor is more observable. The altimeter bias estimation error is also shown in Figure 4-8. The vehicle descends to 10,000 feet at 400 sec. At this low altitude the scale factor effect is less and the bias becomes more observable. The bias uncertainty is reduced to about 200 feet.

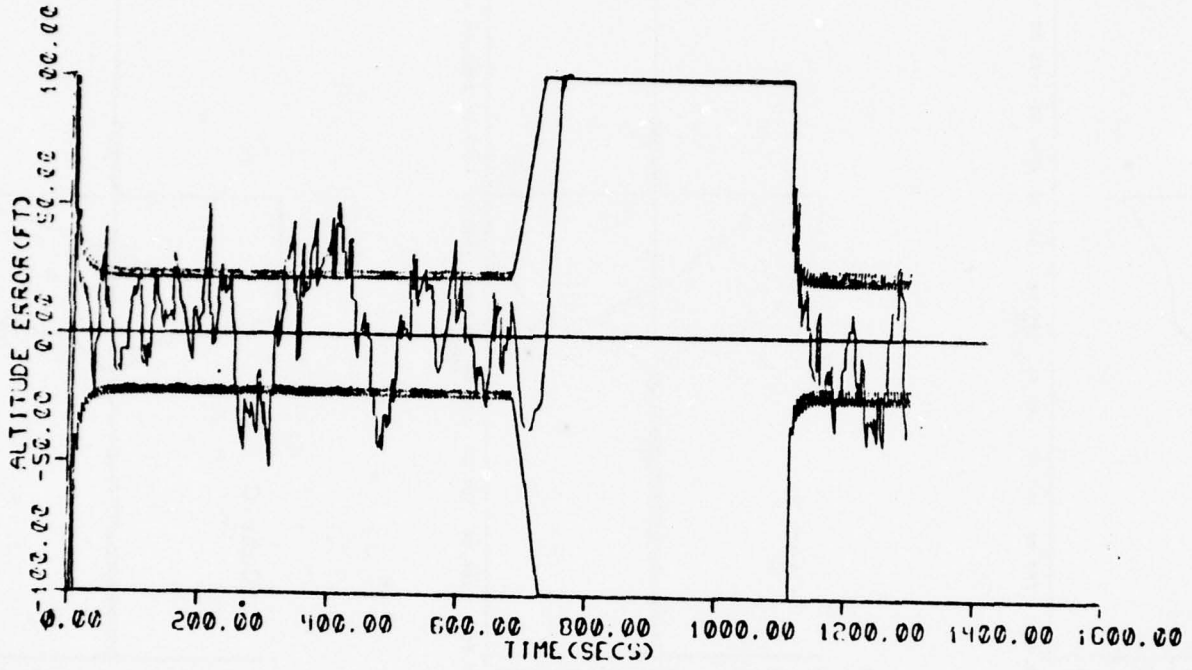

Figure 4-5 GPS/Inertial Altitude Errors for Case A (Expanded Scale)

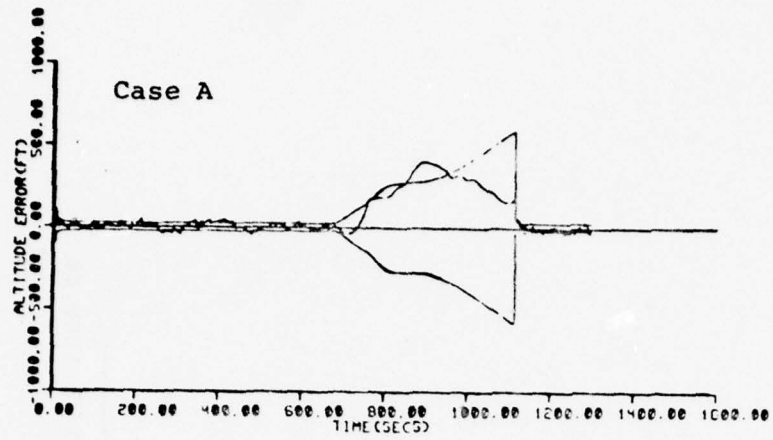

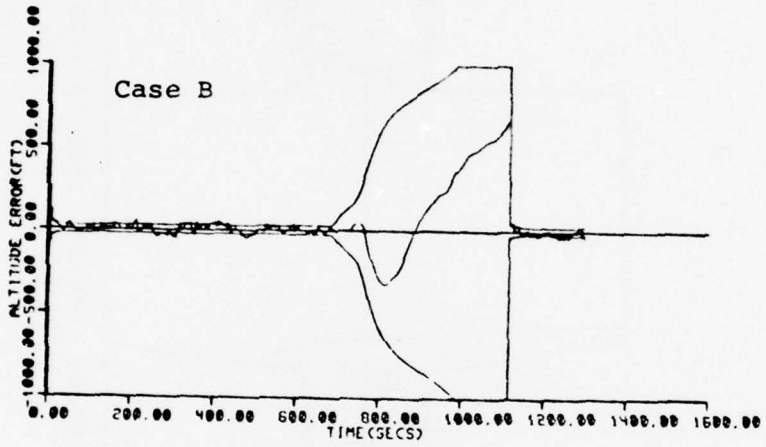

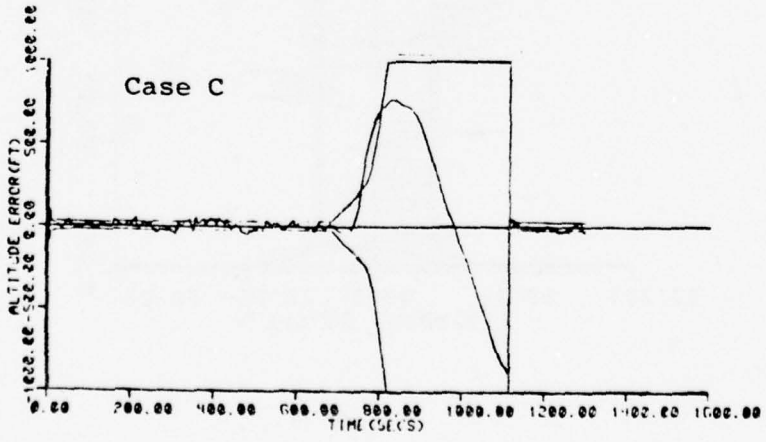

Figure 4-6 GPS/Inertial Altitude Errors

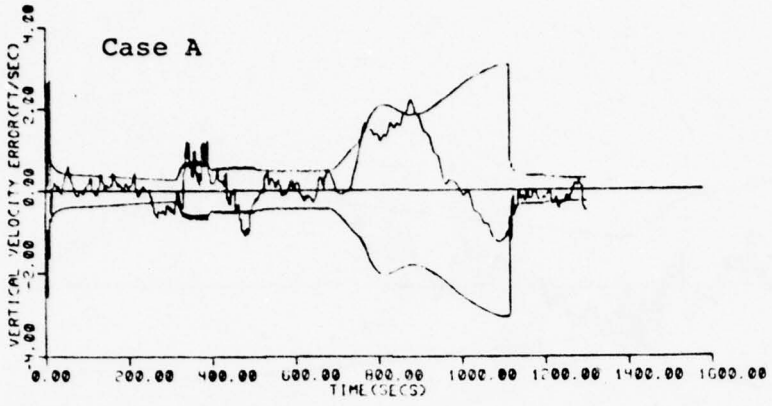

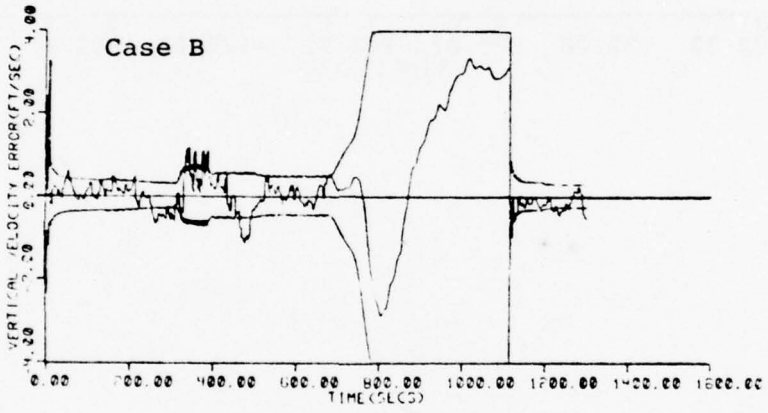

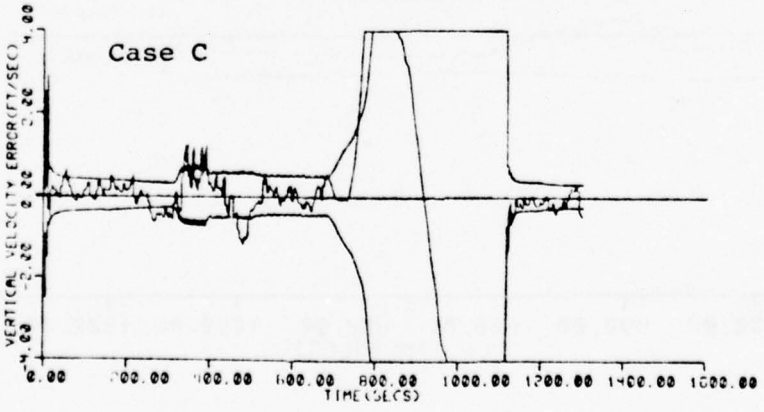

Figure 4-7 GPS/Inertial Vertical Velocity Errors

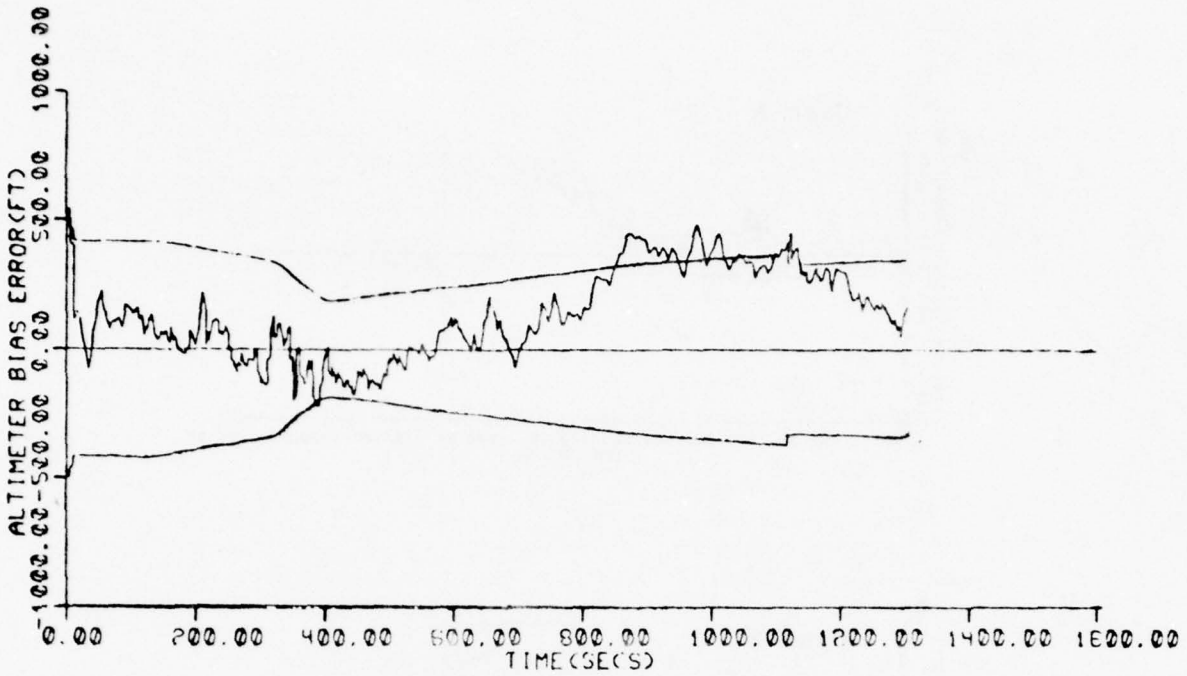

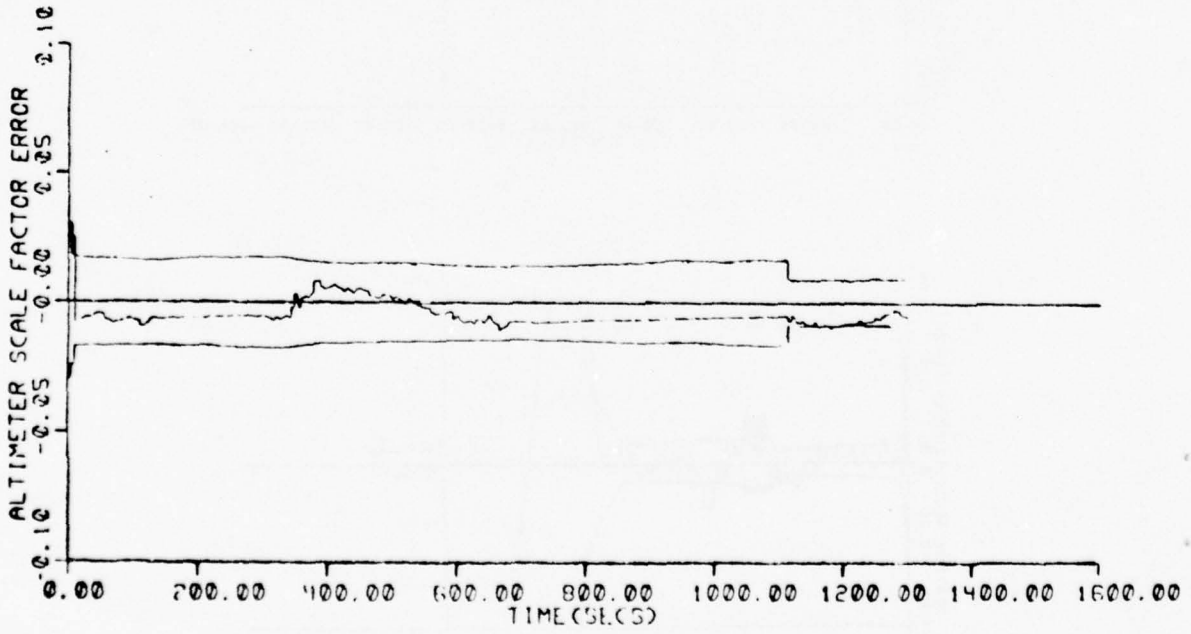

Figure 4-8 Filter A Altimeter Bias and Scale Factor Errors

The first-order Markov altimeter bias simulation in the truth model has a particularly large bias excursion during the period of jamming. Supposedly having a one-sigma value of 500 feet, the bias actually exceeds 1,000 feet. Table 4-1 compares the true altimeter bias with the filter estimate at several points during the period of no GPS signals.

Table 4-1

Altimeter Bias True Values and Filter Estimates - Case A

TIME (SECS)	TRUE VALUE (FT)	FILTER ESTIMATE (FT)	ERROR (FT)
700	785	795	-10
800	914	752	162
900	1084	711	370
1000	1067	673	393
1100	989	636	353

The growth in estimation error to 390 feet is due largely to the 300 foot shift in the true altimeter bias in 300 sec. Such a rapid shift is not realistic for normal weather conditions.

The Case B filter uses a random walk bias state altimeter error model. The estimation error of this state and its filter-computed uncertainty are plotted in Figure 4-9. The estimation error that is plotted is defined to be:

$$\delta e_{bh} = e_{po} + e_{hsf}\, h - e_{bh} \qquad (4\text{-}3)$$

where e_{po} is the truth model altimeter bias, e_{hsf} is the truth model altimeter scale factor error, and e_{bh} is the filter altimeter error estimate. A better definition of the estimation error would have included as well a third term and fourth term from the truth model which are the altimeter error contributions of the static pressure measurement error and the altimeter lag. The static pressure

measurement error contributes about 100 feet of error to the altimeter error at the speeds of this trajectory. Omitting this effect from the estimation error definition of Eq.(4-3) leaves a bias of about 100 feet in the estimation error plot of Figure 4-9.

During the period of GPS signal loss, the filter holds its estimate e_{bh} of altimeter error at a constant value of 1,466 feet. The variations in the estimation error are due entirely to variations in the first two terms of Eq.(4-3). The effects of the reduction in the scale factor error term during the dive at about 750 sec and the growth in that term during the subsequent climb are clearly seen in the estimation error. Note the filter-computed uncertainty for the altimeter error estimate increases during the dive in good agreement with the growth in estimation error. The maneuver dependent filter driving noise, which was given in Eq.(3-16), is working as intended. In the subsequent climb, the filter-computed uncertainty increases further and becomes conservatively large. The single error state model is not able to predict the reduction in the estimation error as the aircraft climbs back to the altitude of the beginning of the period of signal loss.

The Case C filter uses a random walk scale factor single state altimeter error model. The estimation error of this state and its filter computed uncertainty are plotted in Figure 4-10. The estimation error that is plotted is defined to be:

$$\delta e_{seff} = e_{po}/h + e_{hsf} - e_{seff} \qquad (4\text{-}4)$$

where e_{po} and e_{hsf} are from the truth model as before, and e_{seff} is the filter effective scale factor error estimate. The filter state tracks well during the periods of continuous GPS coverage. During the loss of GPS signals, the state holds constant at an estimated effective scale factor error of 0.079. The scale factor error e_{hsf} in the truth model is constant at 0.030, so variations in the plotted estimation error are due to variations in e_{po} or h, which comprise the first term of Eq.(4-4). The dive at about 750 sec drives the first term off scale. The filter-computed uncertainty increases significantly during the dive in accordance with the maneuver dependent driving noise,

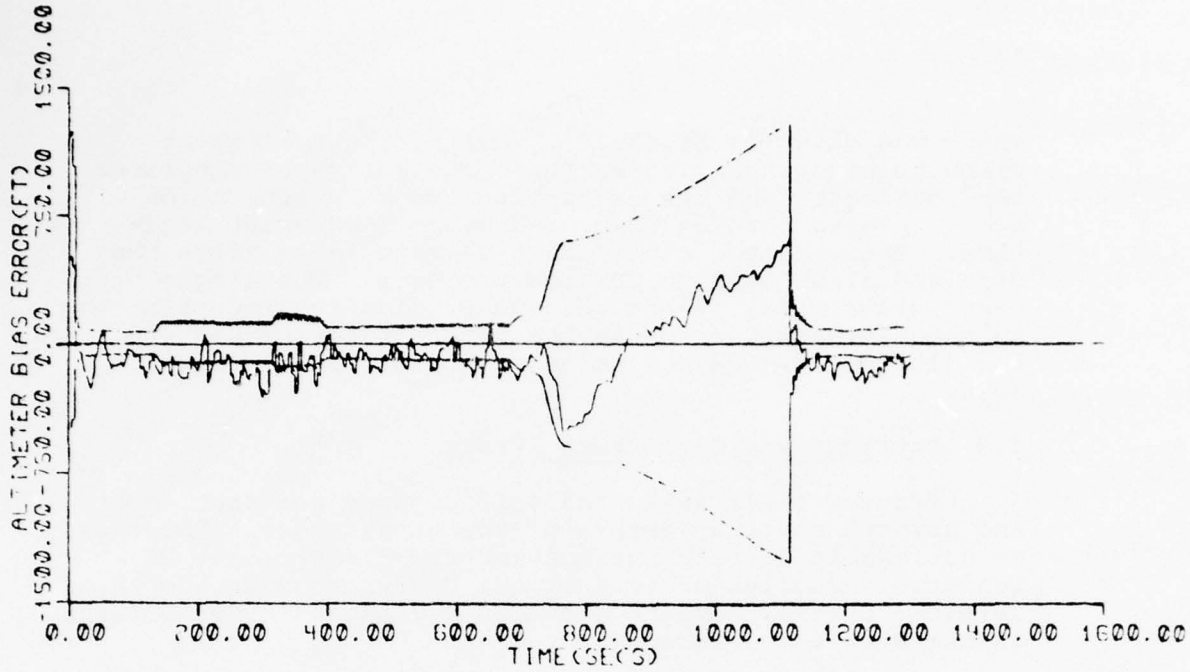

Figure 4-9 Filter B Altimeter Bias Error

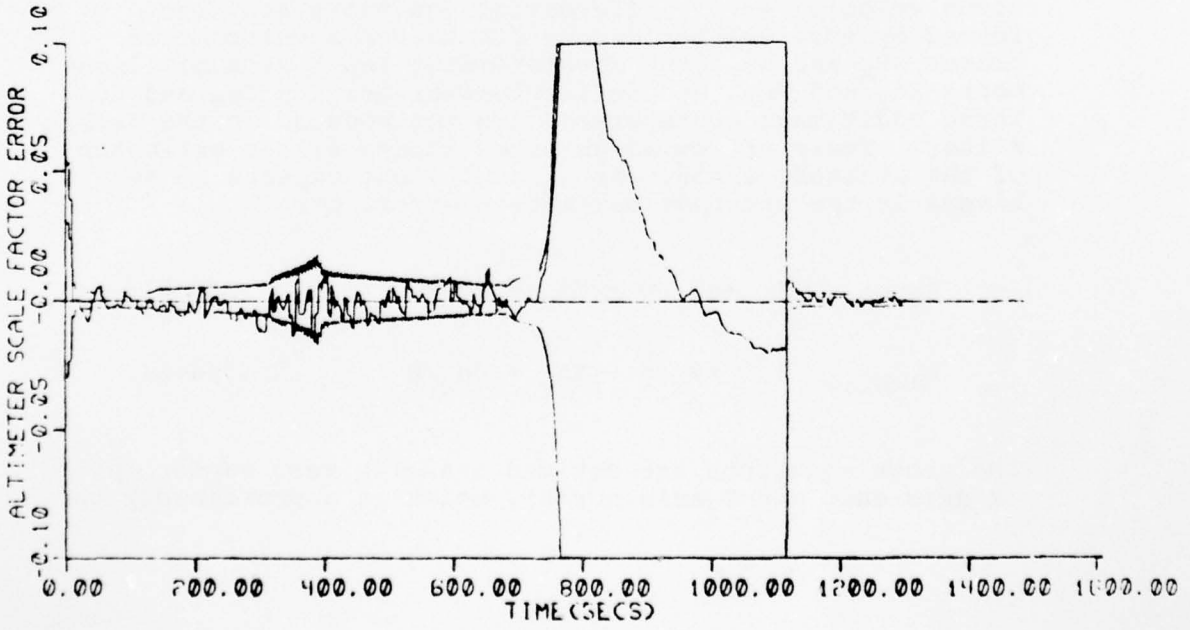

Figure 4-10 Filter C Altimeter Effective Scale Factor Error

which was given in Eq.(3-27). During the subsequent climb to highest altitude, the contribution of the first term decreases and the estimation error returns to on scale, passes through zero, and becomes somewhat negative. The computed uncertainty is very large after the dive and climb with no GPS measurements. The single error state model is not able to predict the reduction in the estimation error as the aircraft climbs back to the altitude of the beginning of the period of signal loss.

4.3 Attitude and Gyro Drift Errors

Figures 4-11, 4-12, and 4-13 compare the east, north, and azimuth attitude errors of the three cases. There are no noticeable differences between the three cases. A reasonable conclusion is that the differences in the three vertical channel designs produce only second order effects in the attitude errors.

Both the east and north components of attitude error are seen to have biases which lie outside the filter computed one-sigma uncertainty. Here this is not an indication of poor filter performance. The attitude estimation error plotted is the difference between the attitude error in the truth model and the attitude error estimate in the filter. The horizontal components of attitude error ε_e and ε_n in the truth model are not the only sources of horizontal acceleration error. Inspection of Table 2-2 giving the truth model fundamental matrix shows that the east and north velocity error differential equations are also forced by acceleration errors due to the accelerometer biases AB_x and AB_y, the accelerometer input axis misalignments XA_y and YA_x, and deflections of gravity δg_e and δg_n. These additional truth states are not modeled in the Kalman filter. Their effect is absorbed in the filter estimates of the attitude error. As a result, one expects to see biases in the attitude estimation errors of:

$$\varepsilon_{e\ bias} \simeq -AB_y/g - YA_x - \delta g_n/g \qquad (4\text{-}5)$$

$$\varepsilon_{n\ bias} \simeq AB_x/g - XA_y + \delta g_e/g \qquad (4\text{-}6)$$

The above equations are derived assuming zero wander angle (X axis east and Y axis north), which is approximately the

case in this simulation. Substituting the initial numerical values for these sources of error gives expected approximate values for the attitude estimation error biases of:

$$\varepsilon_{e\ bias} \simeq -44 \text{ arc sec}$$

$$\varepsilon_{n\ bias} \simeq +46 \text{ arc sec}$$

These values agree approximately with the biases in the plots.

The filter-computed uncertainties of the east and north attitude estimation error show the initial transient and the effect of the maneuver dependent driving noise. During the initial period of non-maneuvering flight, the filter-computed uncertainty is reduced to less than ten arc sec. When the rapid maneuvering begins, the filter-computed uncertainty rises to a higher level.

The azimuth estimation error is shown in Figure 4-13. During the initial period of non-maneuvering flight, the azimuth error is growing and the filter-computed uncertainty shows little improvement. The subsequent maneuvering provides more direct observability of the azimuth error. The estimation error and the computed uncertainty both are reduced.

We have inspected the print-out associated with the gyro drift rate estimates. The results show no reduction in filter-computed uncertainties of the gyro drift rates and the filter estimates of the gyro drift rates remain near the initial zero values. These states therefore were of little benefit to the navigation performance in this flight. It is possible that on a longer flight and with less maneuvering, the filter could obtain a useful estimate of the effective north gyro drift rate and perhaps the azimuth gyro drift rate. In any case, the effective east gyro drift rate is probably unobservable.

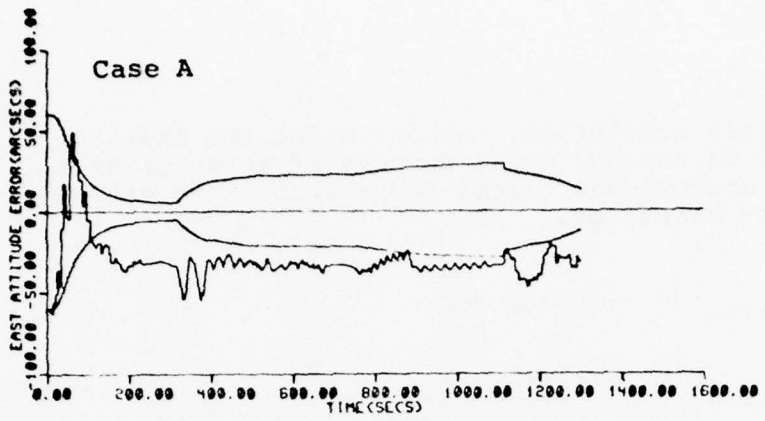

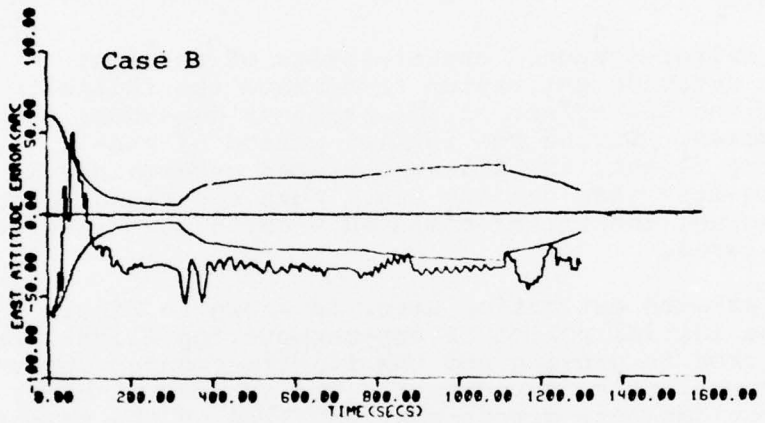

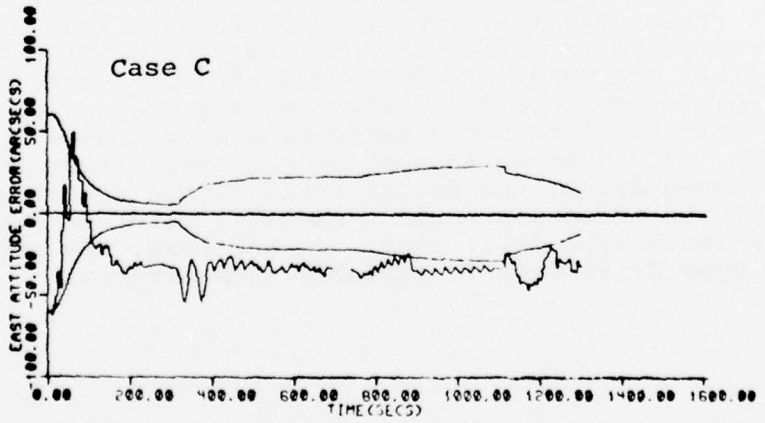

Figure 4-11 GPS/Inertial East Attitude Errors

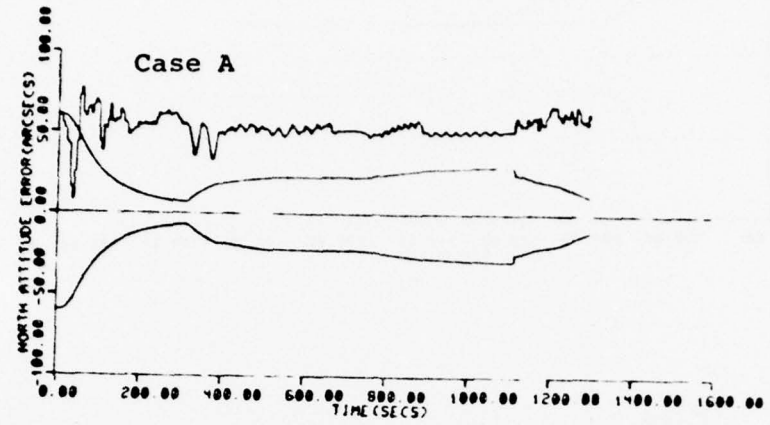

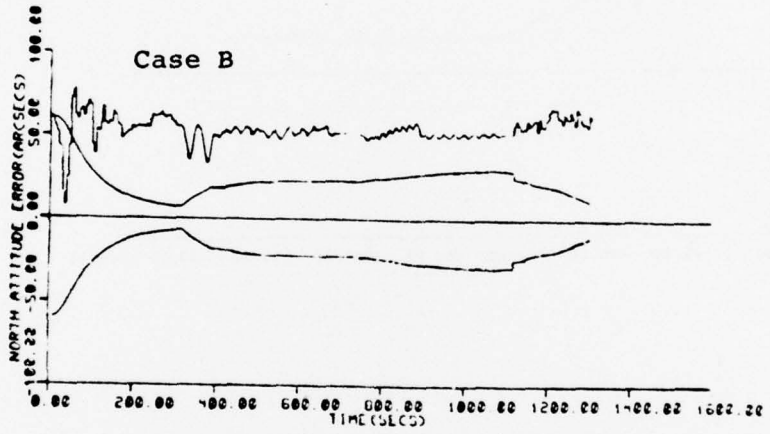

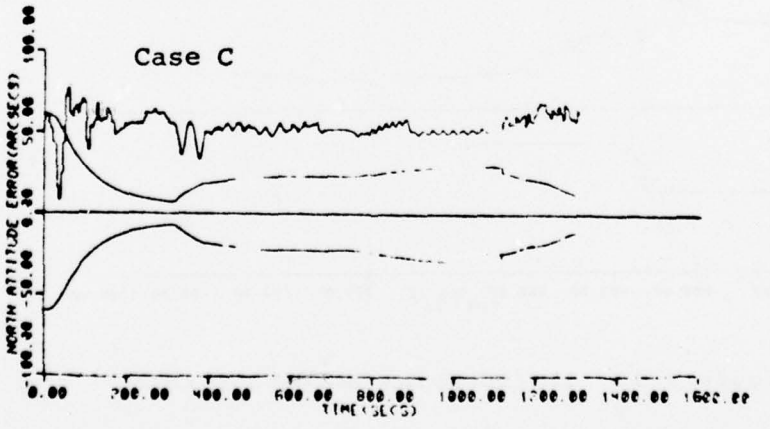

Figure 4-12 GPS/Inertial North Attitude Errors

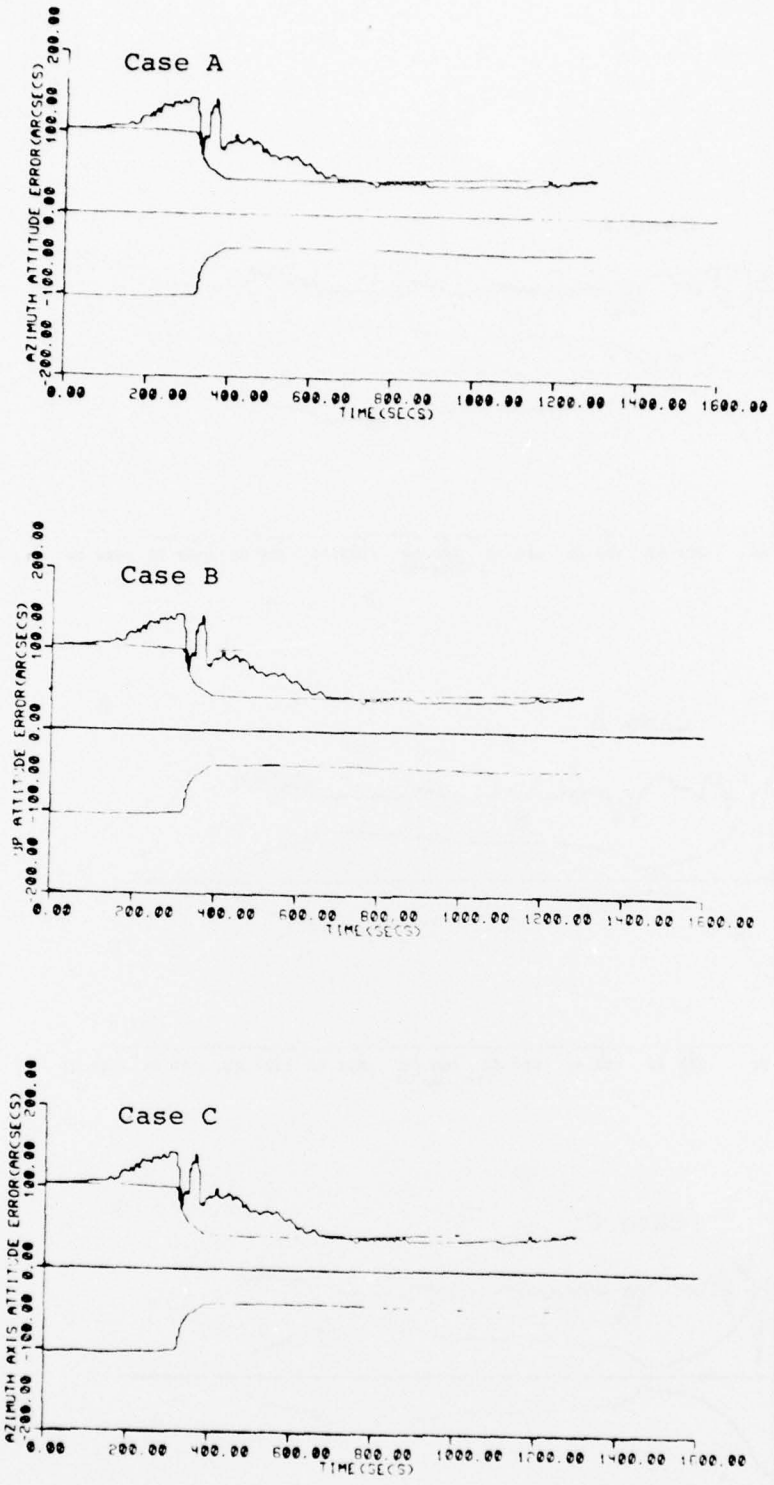

Figure 4-13 GPS/Inertial Azimuth Errors

4.4 Clock Phase and Frequency Errors

Figure 4-14 and 4-15 compare the clock phase and frequency estimation errors of the three cases. There are no noticeable differences between the three cases.

The filter-computed uncertainties for both clock phase and frequency are in good agreement with the level of the estimation errors, both during the periods of GPS measurements and during the jamming period.

Figure 4-16 replots the clock phase error for Case C on an expanded scale. It is interesting to note that the clock phase estimation error is similar (but with a sign reversal) to the altitude estimation error shown in Figure 4-5. This is often observed in GPS navigation solutions. Because the four satellites being used are necessarily above the horizon, the measurement directions are all in the upper hemisphere, which leads to strong correlation between altitude error and clock phase error.

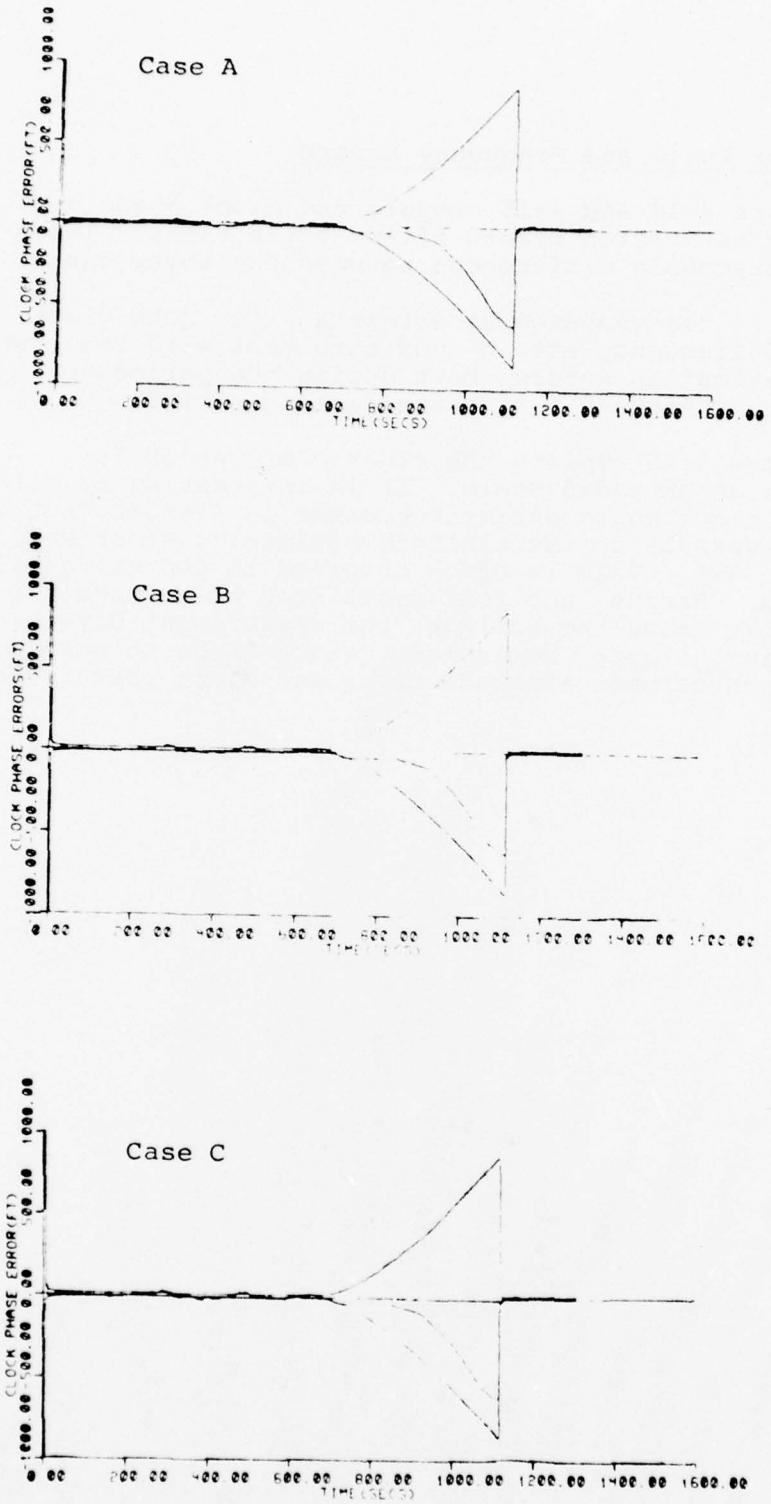

Figure 4-14 Clock Phase Errors

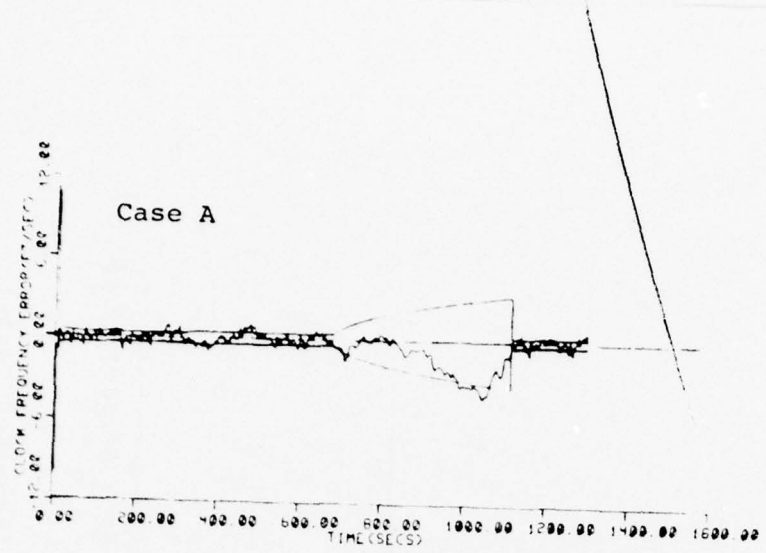

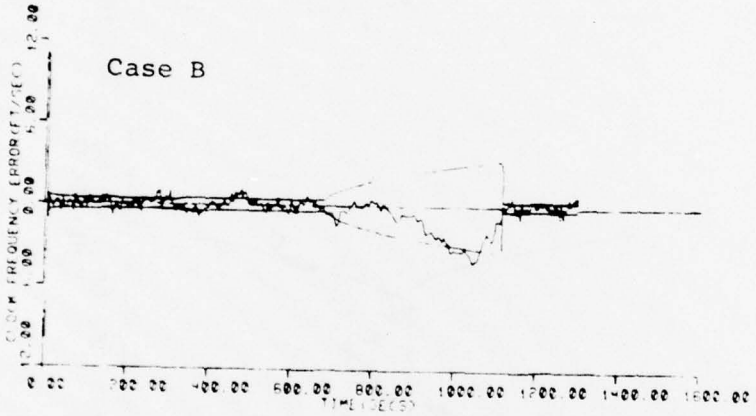

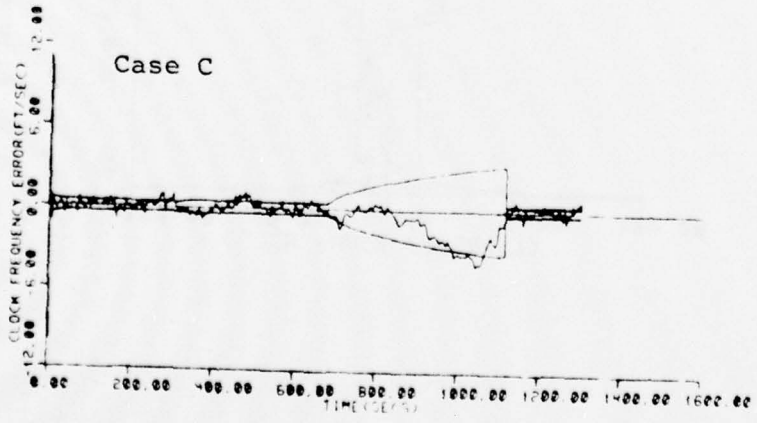

Figure 4-15 Clock Frequency Errors

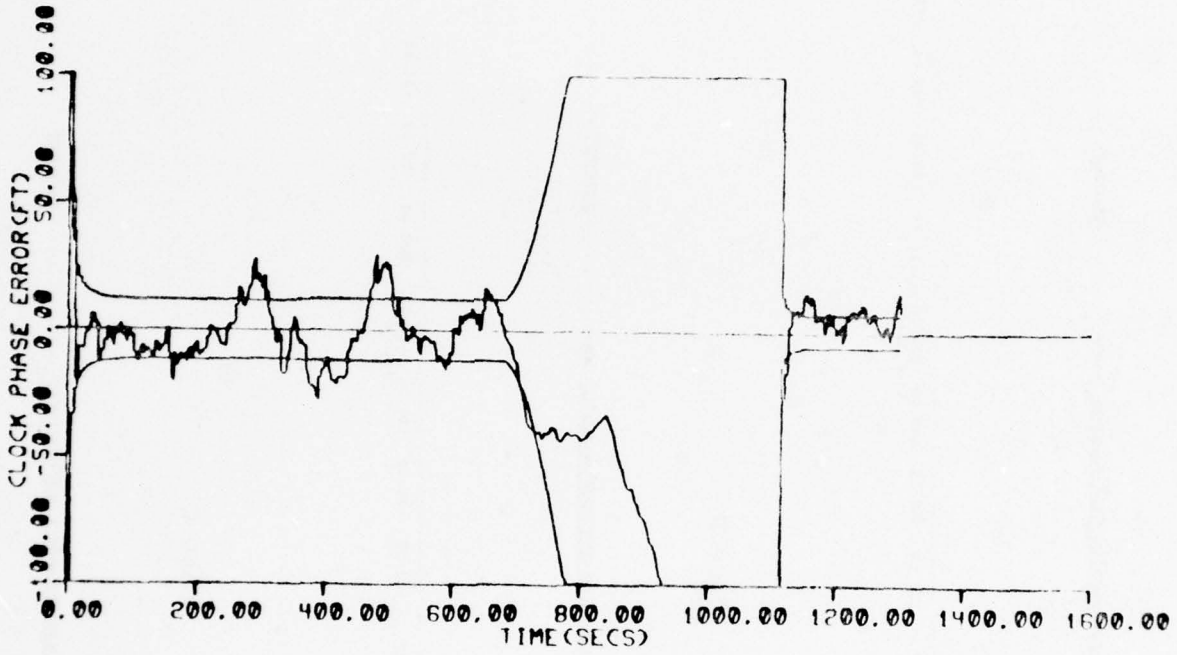

Figure 4-16 Clock Phase Errors for Case C (Expanded Scale)

SECTION V

SUMMARY AND CONCLUSIONS

The Integrated GPS/Inertial (IGI)Simulator has been utilized to explore several design issues associated with the vertical channel of a GPS/baro/inertial navigation system. The primary issues explored were associated with the modeling of barometric altimeter error in the Kalman filter. Should two-state variables be used in the filter to model altimeter error, or is one sufficient? If only one state is used, should it be a bias-like error model or should it be a scale-factor error model? How can an assumed white noise driving a single error state be used to model the effect of other sources of error?

The assumed navigation system is comprised of: a local-level wander azimuth inertial navigation system with associated barometric altimeter for stabilizing the vertical channel, a GPS pseudo range and range-rate receiver, and a navigation computer hosting a Kalman filter to integrate the baro/inertial and GPS data.

The error model in the simulator has fifty-four states representing the inertial navigation position, velocity, and attitude errors, the gyro sources of error, the accelerometer sources of error, the gravity deflections and anomaly, the barometric altimeter sources of error, and the GPS receiver clock phase and frequency errors. Significant sources of barometric altimeter error included are the zero-setting error, the scale factor error, the static pressure measurement error, and the altimeter lag.

The simulated flight path is representative of a F-4 aircraft tactical mission profile. There are periods of straight and level flight, dives and climbs, and high-g evasive maneuvering. There is a seven minute period during which jamming prevents the use of GPS measurements. During this period, the aircraft

dives 15,000 feet to a hypothetical target area, then climbs back to altitude.

Three Kalman filter vertical channel designs were evaluated. Filter A has seventeen states and filters B and C have sixteen states. The first fifteen states are common to all three filters. These are the states modeling INS position, velocity, and attitude errors (9); receiver clock phase and frequency errors (2); gyro drift rates (3); and vertical acceleration error (1). The modeling of these fifteen states is similar to that in the Kalman filter in the original IGI simulator, except that maneuver-dependent variances of the driving noises have been introduced to model the effects of accelerometer scale factor errors and input axis misalignments and to model the effects of gyro g-sensitive drift rates.

Filter A has two states representing the altimeter sources of error: one state a bias error and the other state a scale factor error. Filter B has only one altimeter error state, and it is a random walk bias model. Filter C also has only one altimeter error state, but it is a random walk scale factor error model. The single-state error models have variances for their driving noises that are functions of the altitude changes.

Analysis of the alternate designs, including the comparative simulation results has led to several observations and conclusions. The three filter designs provide essentially identical navigation performance when GPS measurements are available. The differences in performance arise during loss of signal.

Filter A with its two-state altimeter error model provides the best vertical channel performance during loss of signal. After processing external (GPS) measurements during descents and climbs, the filter is able to calibrate both the zero-setting error and the scale factor error. This leads to improved vertical channel performance during the subsequent dive and climb in the period of no external measurements (jamming). In the jamming period, peak altitude error was 400 feet and the largest vertical velocity error was about two feet per second.

Filter B with its single-state altimeter bias model

converges to a correct estimate of the combined altimeter error while processing external measurements. During the jamming period, the bias estimate holds constant. In the dives and climbs during the jamming period, the true altimeter scale factor error causes shifts in the altimeter error, which cannot be compensated by filter B. The simulation results exhibited altitude errors from -340 to 680 feet and a peak vertical velocity error of about 3 feet/sec.

Filter C with its single-state altimeter scale factor model has the worst vertical channel performance. The estimate of the effective scale factor error converges to a correct value while processing external measurements. This effective scale factor error estimate when multiplied by the current altitude gives a value for baro altitude error that matches the total baro altitude error from the several sources of error. During the jamming period, the effective scale factor error estimate holds constant. The accuracy of the baro altitude error estimate, during dives and climbs in this jamming period, depends on the difference between the estimated effective scale factor error and the true scale factor error. In the simulation case, the estimated scale factor error was 0.08 and the true scale factor error was 0.03. The difference of 0.05 provided a strong excitation to the errors in the filter estimates of vertical velocity and altitude. Altitude errors ranged from 770 feet to -885 feet and the peak vertical velocity error was larger than 4 feet/sec. The vertical velocity estimation errors of the filter were actually larger than the vertical velocity errors of the no-filter baro-inertial system. If the period of jamming had started at a higher altitude or had the zero setting error been smaller, then the difference between the effective scale factor error and the true scale factor error would have been smaller and the subsequent vertical channel errors during the dives and climbs would have been smaller.

A filter similar to filter C was evaluated by Myers and Butler. It also had a single-state altimeter error model, which was a scale factor error. However, this state was modeled as a random constant rather than a random walk. In the simulation results, while processing GPS measurements (no jamming) the filter diverged from correct estimates of vertical

velocity, altitude, and even latitude and longitude. While we have not attempted to re-run this exact design, we believe the design diverged because of the random constant model. With such a model, the filter will converge to a fixed estimate of the effective scale factor error and the computed uncertainty will go to zero. With complete confidence in its calibrated baro altimeter data, and because of the closed baro-inertial loop, the filter computed uncertainty in the estimate of altitude also goes to zero. The filter then ignores current external (GPS) measurements as far as altitude updating is concerned. If there is actually a large altitude estimation error, the GPS measurement residuals must be put somewhere, and this leads to forced errors in the estimates of latitude, longitude, and clock phase. The filter C evaluated in this report avoids these performance difficulties by using a random walk error model. The variance assigned to the driving noise is sufficient to prevent the filter from becoming over confident.

The other estimation errors of the three Kalman filter designs were also analyzed. The horizontal position and velocity errors, the attitude errors, and the clock phase and frequency errors for the three cases were essentially identical including during the period of jamming. The differences in the vertical channel designs produced no significant differences in these other errors.

The three filters exhibited good self consistency. The filter computed uncertainties were generally in agreement with the estimation errors. An exception was the north position error, which had a bias value exceeding the computed uncertainty. Changes to the measurement processing are proposed which should eliminate the bias. The horizontal components of attitude error also have values exceeding the computed uncertainties. These biases are the unobservable tips due to various sources of horizontal acceleration measurement error. The maneuver dependent driving noises for the velocity error states, the attitude error states, and the baro altitude error state help provide the desired consistent performance.

REFERENCES

1. Myers, K. A., and Butler, R. R., "Simulation Results for an Integrated GPS/Inertial Aircraft Navigation System", presented at the National Aerospace Electronics Conference, Dayton, Ohio, 18-20 May 1976.

2. Widnall, W. S., and Grundy, P. A., "Inertial Navigation System Error Models", Report TR-03-73, Intermetrics, Inc., Cambridge, Mass., 11 May 1973.

3. Myers, K. A., "Integrated GPS/Inertial (IGI) Direct Simulation State Propagation Approach", RWA-3 Tech Memo, AFAL/WPAFB, Dayton, Ohio, 1 August, 1975.

4. Widnall, W. S., Carlson, N. A., and Grundy, P. A., "Post Flight Processor for CIRIS", Report TR 16-72, Intermetrics, Inc., Cambridge, Mass., 24 November 1972.